ANNUAL REVIEWS

Annual Review of Astronomy and Astrophysics

Atmospheres of Rocky Exoplanets

Robin Wordsworth[1] and Laura Kreidberg[2]

[1]School of Engineering and Applied Sciences and Department of Earth and Planetary Sciences, Harvard University, Cambridge, Massachusetts, USA; email: rwordsworth@seas.harvard.edu

[2]Max Planck Institute for Astronomy, Heidelberg, Germany

Annu. Rev. Astron. Astrophys. 2022. 60:159–201

First published as a Review in Advance on April 28, 2022

The *Annual Review of Astronomy and Astrophysics* is online at astro.annualreviews.org

https://doi.org/10.1146/annurev-astro-052920-125632

Keywords

exoplanets, atmospheres, planet formation, chemistry, habitability, biosignatures

Abstract

Rocky planets are common around other stars, but their atmospheric properties remain largely unconstrained. Thanks to a wealth of recent planet discoveries and upcoming advances in observing capability, we are poised to characterize the atmospheres of dozens of rocky exoplanets in this decade. The theoretical understanding of rocky exoplanet atmospheres has advanced considerably in the last few years, yielding testable predictions of their evolution, chemistry, dynamics, and even possible biosignatures. We review key progress in this field to date and discuss future objectives. Our major conclusions are as follows:

- Many rocky planets may form with initial H_2–He envelopes that are later lost to space, likely due to a combination of stellar UV/X-ray irradiation and internal heating.
- After the early stages of evolution, a wide diversity of atmospheric compositions is expected as a result of variations in host star flux, atmospheric escape rates, interior exchange, and other factors.
- Observations have ruled out both the presence of H_2-dominated atmospheres on several nearby rocky exoplanets and the presence of any thick atmosphere on one target. A more detailed atmospheric characterization of these planets and others will become possible in the near future.
- Exoplanet biosphere searches are an exciting future goal. However, reliable detections for a representative sample of planets will require further advances in observing capability and improvements in our understanding of abiotic planetary processes.

Contents

The Spirits answered, That there were more numerous Worlds than the Stars which appeared. . . .

—Margaret Cavendish, *The Blazing World* (1688)

1. INTRODUCTION

Hot Jupiter: a gas giant planet that orbits close to its host star and hence has an extremely hot atmosphere

While speculation on the nature of planets around other stars goes back for centuries, exoplanet science is a young discipline, having begun in earnest only in 1995 with the discovery of the hot Jupiter 51 Pegasi b (Mayor & Queloz 1995). The 27 years since this discovery have seen rapid improvements in instrumentation and observing techniques. These improvements have in turn led to major advances in our understanding of planet formation, the abundance of different planet types around different stars, and the atmospheric compositions of gas-rich planets very different from those in the Solar System. Thanks to a combination of ground- and space-based observations, we also know of hundreds of planets that have around the same radius as Earth (Batalha et al. 2013). Most of these planets are distant from the Solar System, but a handful of them are close enough to allow more detailed characterization. Some of them may host life.

Since the first exoplanet discovery, it has been clear that technological advances would eventually allow us to study the atmospheres of these low-mass planets. In anticipation, increasing theoretical attention is now devoted to predicting the composition, circulation, chemistry, and climates of rocky exoplanets. In the last few years alone, the very first observational constraints on rocky exoplanet atmospheres have begun to emerge, and major new steps forward are expected in the near future.

The motivation for studying rocky planets around other stars is immense. Despite everything we have learned from Earth, Mars, and Venus, it is not possible to create a general theory of atmospheres by studying a handful of objects, each of which is very different from the others. Earth, in particular, is unique. No other Solar System planets have surface liquid water or, to the best of our knowledge, life. Why is this the case? What determines the distribution of water and other volatiles on rocky planets generally? When do rocky planets retain atmospheres, and why? How does a planet's chemistry affect its evolution, including its chances of developing a detectable biosphere? All these questions were speculative until recently, but in the next few years we will be able to tackle them directly.

Observations of rocky planet atmospheres pose a major technical challenge, because they are dwarfed in size and brightness by their host stars. The most immediately accessible systems are rocky planets transiting small M-dwarf hosts; for these systems, the expected atmospheric signal is ~10 parts per million relative to the host star brightness. A handful of these planets have already been studied with current telescopes, and more observations in greater detail will be enabled by near-future observing facilities such as the *James Webb Space Telescope* (*JWST*) and 30-meter-class ground-based telescopes (Snellen et al. 2015, Morley et al. 2017). Direct imaging of reflected light spectra of Earth analogs is also a high priority for the exoplanet community, but these signals are even smaller—the contrast between the Earth and the Sun is 10^{-10} in optical light—and will require a next-generation space telescope (Feng et al. 2018, Natl. Acad. Sci. Med. 2018).

This review summarizes major results in the study of rocky exoplanets to date, with a focus on the composition and evolution of their atmospheres. By necessity, our discussion is weighted toward theory, because only a few observational constraints on rocky planet atmospheres currently exist. However, in this decade our view of exoplanet atmospheres will undergo a revolution, thanks to the arrival of *JWST* and the new ground-based telescopes. By summarizing the current state of knowledge, we aim for this review to serve both as an aid for future investigation and as a summary of key predictions of the field ahead of this new wave of observations.

The rest of this review is structured as follows. The next three subsections cover some background and fundamentals. In Section 2 we review the processes that drive atmospheric formation and loss to space. In Section 3 we discuss atmospheric chemistry, including the important topic of redox evolution. We discuss atmospheric exchange with the surface and interior in Section 4 and atmospheric dynamics in Section 5. Section 6 reviews all the observational constraints on rocky exoplanet atmospheres obtained to date. Finally, in Section 7 we discuss future prospects for the field, including the exciting question of how we can characterize habitability and search for life on exoplanets.

Volatile: an element or species found predominantly in gaseous form in a given temperature and pressure range

M-dwarf: a star that is relatively small and cool compared with the Sun; M-dwarfs are the most common type of star in the Milky Way galaxy

1.1. What Is a Rocky Planet?

In the Solar System, the distinction between rocky planets and gas/ice giants is obvious: Mercury, Venus, Earth, and Mars are rocky, while Jupiter, Saturn, Uranus, and Neptune are giants. However, a major contribution of exoplanets to planetary science so far has been to show us that this neat Solar System distinction does not hold true in general. In fact, planets intermediate in size between Earth and Neptune are an abundant outcome of planet formation (Howard et al. 2012).

Categorizing these worlds is a challenge. Are they scaled-down versions of Neptune, water-rich worlds, or relatively dry rocky planets surrounded by puffy H envelopes?

Phase curve: a time-series observation of a planet over its entire orbit

Mass and radius measurements can provide useful guidance about the bulk composition of a planet—most notably, the addition of H rapidly increases the radius for a given mass (Valencia et al. 2010). This information has been widely used in the exoplanet literature to separate rocky and nonrocky planets, in the absence of any observational constraints on their atmospheric properties (e.g., Rogers 2015). Following this approach, we consider a planet rocky if its mass and radius are consistent with that of a bare rock, within typical observational uncertainties for exoplanets (10% precision on the mass, 5% precision on the radius). The upper bound on the radius of a rocky planet is then set by the mass–radius relation for a pure silicate ($MgSiO_3$) composition, and the lower bound is set by a pure Fe composition. Most rocky bodies are expected to be composed of Fe cores and silicate mantles and therefore lie between these two extremes.

This definition includes all the terrestrial planets of the Solar System, as even thick atmospheres like that of Venus contribute only ∼1% to the planetary radius at optical wavelengths. The definition also allows for a wide diversity of possible compositions, including ocean worlds that are entirely covered by a water layer, or planets with a small H_2 atmosphere ($\lesssim$0.1% by mass; Lopez & Fortney 2014). It does not include planets with thicker H_2-rich envelopes or tens of percent of water by mass, which we refer to in this article as sub-Neptunes. As we discuss in Section 2, some small H_2-rich exoplanets may share a common origin with rocky planets (see also Bean et al. 2021 for a recent review).

Figure 1 shows the mass–radius relation for exoplanets and the Solar System. Planets below roughly 1.6 Earth radii ($R_\oplus$) are consistent with a rocky composition (Weiss & Marcy 2014, Rogers 2015, Wolfgang & Lopez 2015). At larger radii, there is much more scatter in the mass–radius relation, with most (but not all) planets requiring a significant mass fraction of volatiles. Exoplanets in the 1.5–2.0 $R_\oplus$ radius range are less abundant than those of lower or higher radius, most likely because of the rapid increase in radius that occurs once an H_2 envelope is present. This phenomenon has come to be known as the radius gap (Fulton et al. 2017, Van Eylen et al. 2018).

1.2. Key Techniques for Observing Exoplanet Atmospheres

Several general approaches are used to measure the tiny signals from rocky planet atmospheres (summarized in **Figure 2**). One is time based: We can monitor the combined flux from the star and planet over time in order to search for variation in brightness as the planet's viewing geometry changes. The most common time-based method is transmission spectroscopy, which consists of a series of spectra measured over the course of a planet's transit. During the transit, a small fraction of the stellar light is transmitted through the planet's atmosphere, where it can be absorbed or scattered. In addition to transit spectroscopy, the planet can be observed at other times during its orbit. During secondary eclipse, all of the thermal emission and reflected light from the planet are blocked by the star, and the planet signal can be inferred from the missing light. The planet can also be observed over its entire orbital period (a so-called phase curve), where different phases of the planet are observable over time. These measurements can be made at low spectral resolution to reveal broad molecular absorption bands. Alternatively, the atmosphere can be observed at high resolution ($R \sim 100{,}000$), which spectrally resolves individual absorption lines (e.g., Snellen et al. 2010). High-resolution spectra are typically blended with light from the host star, but the signal-to-noise ratio can be improved with starlight suppression techniques (Lovis et al. 2017).

These combined light measurements require bright, nearby host stars (generally within 15 pc). They are most feasible for planets with small M-dwarf host stars (the smaller the star, the larger the planet signal). They are also best suited to short-period planets, which are statistically more likely

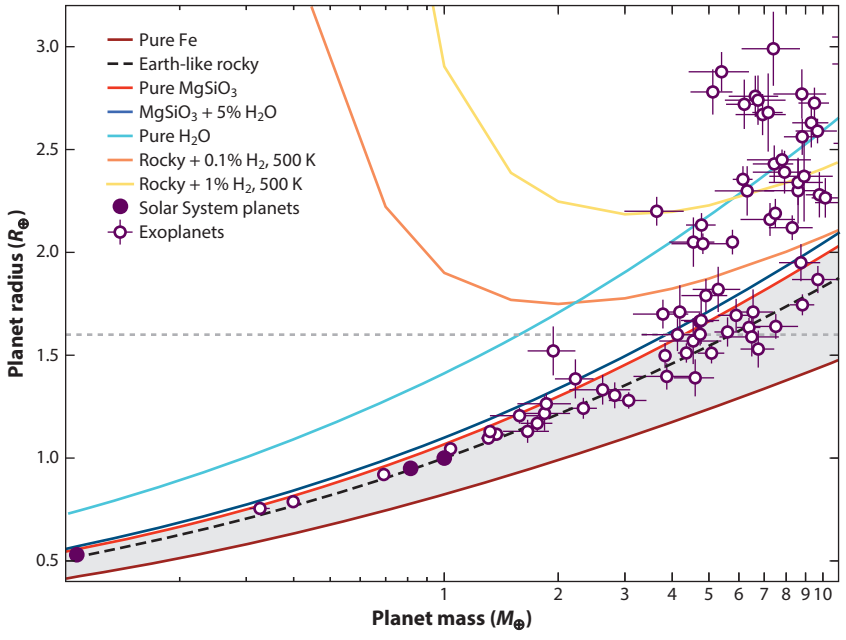

Figure 1

Mass and radius measurements for exoplanets and the Solar System planets, compared with model compositions. For clarity, we show only planets with 5σ mass measurements. The gray shaded region indicates the part of parameter space we consider to be rocky, where the mass and radius are consistent with a composition dominated by Fe and/or silicate (here, defined as $MgSiO_3$). The horizontal dotted line marks the threshold suggested by Rogers (2015), above which the majority of planets retain an H_2 envelope. The mass and radius measurements are from the NASA Exoplanet Archive (see **https://exoplanetarchive.ipac.caltech.edu/**), and model compositions are from Zeng et al. (2019).

to transit. **Table 1** lists the 10 most observationally accessible rocky planets for combined light measurements (as of 2021). Of particular note is the TRAPPIST-1 system, which has seven rocky planets transiting an ultracool dwarf star (Gillon et al. 2017). These planets are among the easiest to characterize, enabling detailed comparative study among multiple planets in the same system (Morley et al. 2017, Lustig-Yaeger et al. 2019b). Extensive surveys from the ground and space (e.g., the *Transiting Exoplanet Survey Satellite*; Ricker et al. 2015) have searched a large fraction of the sky with the sensitivity needed to detect such systems, so it is increasingly unlikely that better targets will be found. The targets listed in **Table 1** may therefore be the most accessible transiting planets we will ever know.

Most observational efforts to date have focused on combined light measurements, but to push these efforts to rocky planets that have larger host stars and wider orbits (e.g., Earth analogs), the more promising approach is direct imaging: high-contrast, high-angular-resolution observations that suppress the light from the star by many orders of magnitude. Direct imaging of Earth analogs is beyond the capabilities of current instrumentation, but this is a major goal for future telescopes, as we discuss in Section 7.

1.3. Some Initial Insights from the Solar System

While exoplanets are expected to be highly diverse, much has already been learned about rocky planet atmospheres from the Solar System. **Figure 3** shows a plot of the atmospheric abundances

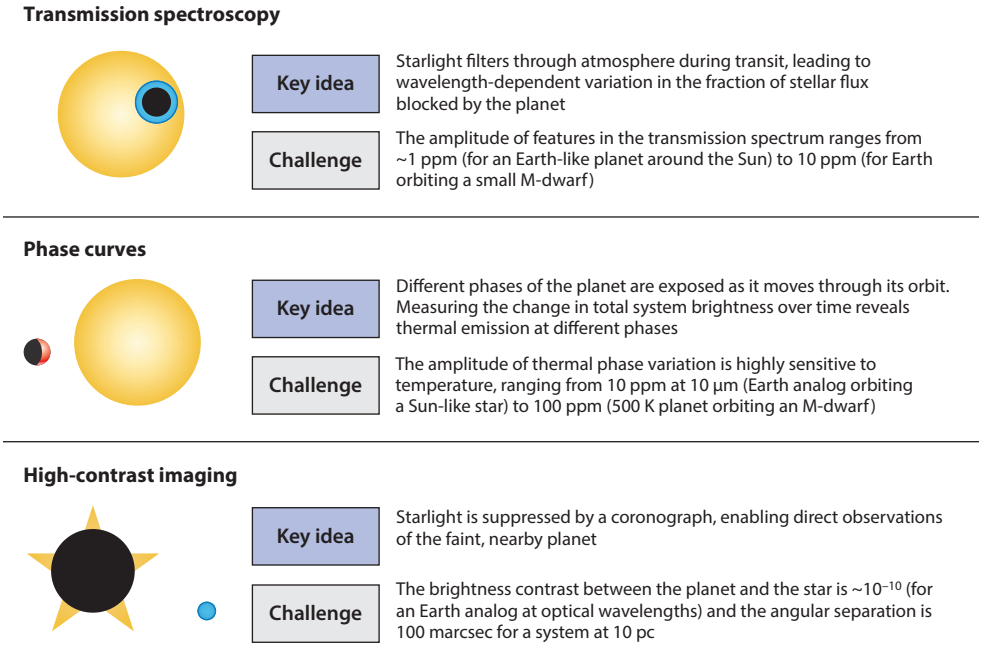

Figure 2

Summary of key techniques for exoplanet atmosphere characterization.

Solar composition gas: a gas mixture with the same elemental abundance ratios as the Sun

of a few key volatile and refractory elements relative to bulk mantle Si for Venus, Earth, Mars, and solar composition gas. A few major trends are immediately obvious. First, Li, Be, B, Na, Mg, Al, and Si are absent from all three terrestrial planet atmospheres. More surprisingly, all three atmospheres are also substantially depleted in volatile elements relative to solar composition: most obviously H and He, but also F, Ne, S, Cl, Ar, and, to a lesser extent, C, N, and O. These underlying elemental

Table 1 System parameters for the rocky planets most accessible for transmission spectroscopy

Planet	R_p ($R_\oplus$)	M_p ($M_\oplus$)	Period (days)	T_{eq} (K)	R_* (R_{sun})	Distance (pc)	TSM
TOI-540 b	0.9	0.7	1.2	611	0.19	14.0	38.8
Gliese 486 b	1.3	2.8	1.5	700	0.33	8.1	35.5
LHS 3844 b	1.3	2.7	0.5	804	0.19	14.9	35.2
LTT 1445 A b	1.3	2.9	5.4	420	0.28	6.9	30.2
GJ 1132 b	1.1	1.7	1.6	529	0.21	12.6	29.3
GJ 357 b	1.2	1.8	3.9	524	0.34	9.4	29.2
TRAPPIST-1 b	1.1	1.0	1.5	399	0.12	12.1	27.6
L 98-59 c	1.4	2.4	3.7	522	0.31	10.6	26.7
LHS 1140 c	1.3	1.8	3.8	438	0.21	15.0	25.2
TRAPPIST-1 d	0.8	0.3	4.0	287	0.12	12.1	24.1
TRAPPIST-1 c	1.1	1.2	2.4	341	0.12	12.1	23.5

The Transit Spectroscopy Metric (TSM) is the normalized signal-to-noise ratio for features expected in the transmission spectrum (Kempton et al. 2018). The equilibrium temperature (T_{eq}) assumes full heat redistribution and zero Bond albedo. The masses of TOI-540 b and LHS 3844 b were estimated from an Earth-like mass–radius relation. The table is based on data from the NASA Exoplanet Archive.

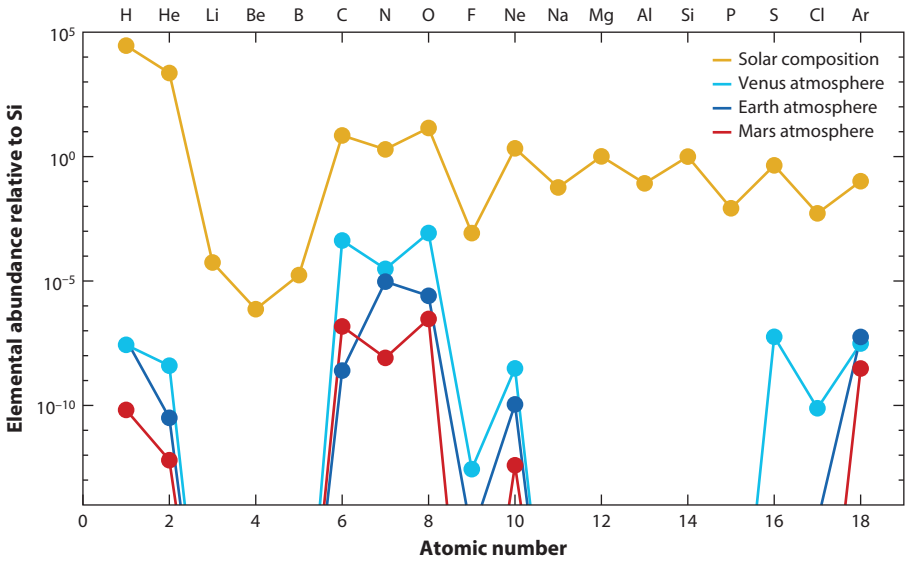

Figure 3

Abundances of low-mass elements in the Solar System, relative to Si, based on values from Lodders (2003), Yung & DeMore (1999), and references therein. For the atmospheres of Venus, Earth, and Mars, abundances are shown relative to mantle Si. The elemental abundance of the Sun is similar to that of nearby stars that host small planets (Buchhave & Latham 2015, Bedell et al. 2018). Atmospheric abundances of some minor elements, such as P on Venus (Greaves et al. 2021, Snellen et al. 2020), remain poorly constrained.

abundances lead to the predominance of a handful of key molecules in each atmosphere: CO_2 for Venus, N_2 and O_2 for Earth, and CO_2 for Mars.

The differences shown in **Figure 3** are due to a combination of formation, loss, and interior sequestration processes. Most notably, the extreme H and He depletion shows that either these gases were never captured from the nebula or they escaped to space early on. Other differences are due to sequestration in the interior. Li, Be, B, Na, Mg, Al, and Si all behave as highly refractory elements in the 150–800 K temperature range. In addition, due to various chemical processes, all three planets are often thought to have large (albeit poorly constrained) inventories of H, C, N, and S in their crusts, mantles, and cores (e.g., Desch et al. 2020). A third major effect is condensation on the surface: H_2O as liquid oceans on Earth and both CO_2 and H_2O as ice deposits on Mars. Finally, Earth's atmospheric composition is strongly affected by the presence of life. Combined, these processes form the basis for predicting the compositions of rocky exoplanet atmospheres.

The thermal structures of Solar System atmospheres vary widely, but there are common themes that are expected to hold true for exoplanets. **Figure 4** shows a schematic of the temperature structure and key physical processes in a typical rocky planet atmosphere. In most cases, there is a lower region (typically at pressures of ~0.1 bar and greater; Robinson & Catling 2014) where convection dominates (the troposphere) and an upper region where convection is inhibited and radiative balance ensues (the stratosphere). Below the troposphere, the highly turbulent planetary boundary layer connects the surface to the lower troposphere. Within the troposphere, temperature declines with altitude due to near-adiabatic behavior of convecting air parcels. In the stratosphere, temperature declines more slowly, and can even increase with altitude due to UV absorption by species such as ozone (**Figure 4**). Above the stratosphere lies the thermosphere, where heating by absorption of extreme ultraviolet and X-ray (XUV) stellar photons makes temperatures highly variable,

Refractory: an element or species found predominantly in solid form in a given temperature and pressure range

Adiabatic: refers to a process in which there is no heat or mass transfer between a system and its environment

XUV: in the planetary literature, defined as the combination of X-ray and extreme ultraviolet radiation (i.e., radiation at all wavelengths below 121 nm)

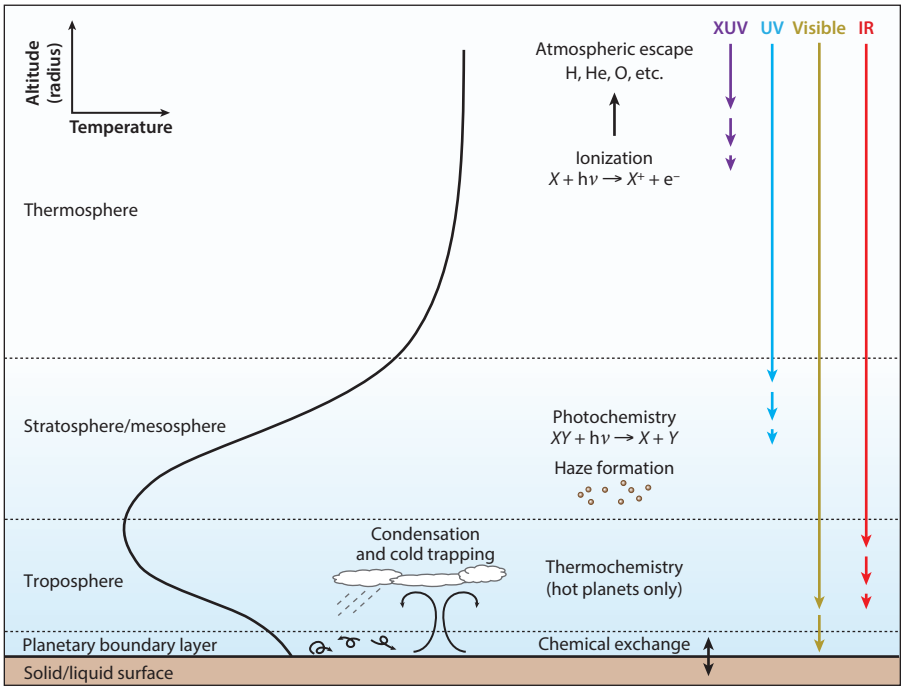

Figure 4

Schematic indicating temperature structure (*solid black line*), key physical processes and transparency to XUV, UV, visible, and IR radiation in the atmosphere of a rocky planet. Note that thermospheric temperatures vary widely depending on stellar flux and atmospheric composition. Abbreviation: XUV, extreme ultraviolet and X-ray.

increasing up to thousands of degrees Kelvin in some cases. This region is critical to atmospheric escape, as we discuss in Section 2.

In the Solar System, surface pressures are mainly an outcome of slow evolutionary processes and range from 92 bar (Venus) to $<10^{-4}$ bar (Mercury, Pluto). Surface temperatures, in contrast, are largely governed by the interaction of the atmosphere with solar radiation on relatively short timescales via the greenhouse effect. The surface temperatures of rocky planets with atmospheres are almost always greater than their equilibrium temperatures, because most atmospheres are more transparent in the visible than in the IR. As a result, incoming stellar radiation that is absorbed by the surface must be reemitted as IR radiation higher in the atmosphere, giving rise to greenhouse warming (Pierrehumbert 2010b). For thermal radiation in the range of 100 to 5,000 K (i.e., 30–0.6 μm Planck peak), absorption by typical atmospheric species is due to vibrational–rotational transitions within molecules and collision-induced absorption involving multiple atoms and molecules. Homonuclear, diatomic species such as H_2 and N_2 are weak IR absorbers at low abundance, while species such as CO_2, H_2O, NH_3, and CH_4 are strong absorbers, making them effective greenhouse gases. However, even H_2 and N_2 become effective greenhouse gases at pressures above ∼0.1 bar due to collision broadening and collision-induced absorption effects (Goldblatt et al. 2009, Wordsworth & Pierrehumbert 2013a).

Volatile condensation plays a major role in the composition of all planetary atmospheres. Over equilibrium temperature ranges from 39 K (Pluto; Zhang et al. 2017) to 2,700 K (dayside of 55 Cancri e; Demory et al. 2016a), condensables can vary from highly volatile elements

like N in the form of N_2 to relatively refractory elements like Na. Only H_2, He, and Ne can safely be regarded as volatile in all planetary environments. Volatile condensation lets us make broad statements about the atmospheric species permitted for a given equilibrium temperature (Section 7). It also plays a more subtle role in atmospheric chemical evolution via the cold-trap effect (see Sections 2 and 3).

Closely related to volatile condensation is the runaway greenhouse effect. This process, which may be responsible for the divergent climates of Earth and Venus, occurs when a condensable species is also a strong IR absorber (e.g., Ingersoll 1969). It results in a nonlinear transition from a mixed volatile–condensate state to a volatile-only state as a planet's equilibrium temperature increases. For H_2O, the most-studied runaway greenhouse species, the runaway transition occurs at around $T_{eq} = 266$ K (Goldblatt et al. 2013). Runaway greenhouse effects are important for determining atmospheric composition and can also influence a rocky planet's observed radius (Turbet et al. 2020).

2. ATMOSPHERIC ACQUISITION AND LOSS TO SPACE

Formation and loss processes are critical to the evolution of rocky planets over their lifetimes. In this section, we review how atmospheres are acquired during planet formation, and then discuss the processes that drive loss of H and other species to space.

2.1. Atmospheric Capture and Volatile Delivery During Formation

Volatile elements can be delivered to planets in two essential ways: as gases in the protoplanetary nebula or as condensed solids (the latter either in pure form or bound to other elements). In Solar System science, it is common to refer to the atmospheres that result from these two processes as primary and secondary, respectively. Nebular capture occurs when a protoplanet forms before the nebula is dispersed. For gas to remain gravitationally bound to a planet or protoplanet, the temperature of the atmosphere must be low enough that most molecules have kinetic energy E_K lower than their gravitational potential energy E_P. The point at which this happens can be defined in terms of a gravitational escape parameter (sometimes called the Jeans parameter):

$$\lambda \equiv \frac{E_P}{E_K} = \frac{GMm}{kTR}. \quad 1.$$

Here, G is the gravitational constant, M is the planet mass, m is the molecular mass, k is the Boltzmann constant, T is the local gas temperature, and R is the radius of the base of the escaping region (which may be larger than the solid planet radius). When λ is large, as is the case for more massive, cooler objects, atmospheric capture from the nebula is favored.

The mass of gas that is captured is low for small protoplanets with high solid accretion rates, because accretion heats the planet, decreasing λ. When the solid accretion rate is low, the fraction of nebula captured depends on how much the atmosphere has cooled toward an isothermal profile (Hayashi et al. 1979, Lee & Chiang 2015, Owen et al. 2020). At a threshold of roughly 1 M_E, protoplanets surrounded by nebula can accumulate H_2–He envelopes of around 1% of their mass, greatly increasing their radius and converting them from rocky to gas planets, according to our definition in Section 1.1.

Geochemical evidence suggests that some early nebular capture did in fact occur on the Solar System rocky planets, or at least on their building blocks (e.g., Williams & Mukhopadhyay 2019). However, these thin primitive atmospheres were rapidly lost to space shortly after the nebula dissipated (Lammer et al. 2020). For rocky exoplanets, a diverse range of histories is possible. Indeed, many exoplanets in the 1–3 $R_\oplus$ range may represent a population that formed with H_2–He-rich

atmospheres but only later bifurcated due to loss to space (Van Eylen et al. 2018). The fact that the Solar System planets apparently formed too slowly to reach the mass threshold where they could accumulate percent levels of H_2 and become sub-Neptunes before the disk dissipated is quite puzzling. Further modeling, exploration of exoplanet population statistics, and atmospheric characterization will be required to understand this important aspect of Solar System evolution.

In the absence of efficient nebular capture, delivery of volatiles that are incorporated into silicate minerals or condensed as ices provides another way to build rocky planet atmospheres. The latter process begins when volatiles condense in the outer portions of protoplanetary disks according to the local gas temperature. The decline in disk temperature both with distance from the protostar and with time allows snow lines for various volatile species to be defined (Öberg et al. 2011). Broadly speaking, solid bodies that accrete outside the snow line will be volatile rich, while those that accrete inside will be volatile poor.

The H_2O snow line in the Solar System occurred at around 2–4 AU (Morbidelli et al. 2012), but snow lines vary with star type. Around M-stars, the long period of elevated luminosity before the star joins the main sequence (Baraffe et al. 2015) may lead to lower rates of delivery of H_2O to close-in rocky planets compared with the Solar System (Unterborn et al. 2018). However, formation inside a snow line does not preclude the presence of that species on a planet. Earth is not completely dry today, either because H_2O was present in small quantities in its building blocks or because it was delivered from other sources, such as late-accreting planetary embryos (Raymond et al. 2004). In the latter case, the stochastic nature of accretion and variability in planetesimal water content due to radiogenic heating means that high variance in rocky planet initial water content is expected (e.g., Lichtenberg et al. 2019). Planets can also migrate inward from their original formation locations, as may have occurred in the TRAPPIST-1 system (Unterborn et al. 2018).

2.2. Loss of Volatiles to Space: Hydrogen

As soon as the protoplanetary disk disperses, young rocky planets begin to lose their atmospheres to space. Depending on the circumstances, atmospheric loss may slow to negligible rates after a short time, or it may continue for the lifetime of the planet. It can strip away the entire atmosphere, or leave it almost untouched. Therefore, understanding this process is vital to understanding the range of possible outcomes for rocky planets.

All loss processes work by overcoming the force of gravitational attraction that keeps an atmosphere bound to its planet. In hydrodynamic escape, the atmosphere flows outward to space continuously, as a fluid. Hydrodynamic escape is in a sense the reverse of nebular capture, and it becomes important once λ has values of around 10 or lower. For that to happen, a planet's upper atmosphere must be hot. To get a sense of the numbers, for an Earth-mass planet with extended H_2 atmosphere, at a distance of 1.3 $R_\oplus$, the λ value is 10 if the temperature is 1,150 K. Temperatures above 1,000 K appear high compared with, say, Earth's equilibrium temperature of 255 K, but they are quite easily reached in the upper atmospheres of low-mass planets. One major reason is XUV radiation (Zahnle & Walker 1982). Most gases are highly opaque to XUV radiation (**Figure 4**), so it is absorbed high up, where density is low. In H_2-dominated atmospheres, the absorbed radiation cannot be easily reradiated at temperatures below ~10,000 K (Murray-Clay et al. 2009), and conduction to the lower atmosphere is often inefficient (Watson et al. 1981). Therefore, extremely high temperatures and hence low λ values are reached, in turn leading to hydrodynamic outflow to space.

In the limit where most XUV energy is used to drive atmospheric loss to space, an energy-limited mass loss flux can be calculated as follows:

$$\phi_E = \frac{\epsilon F_{XUV}}{4V_{pot}}. \quad 2.$$

Here F_{XUV} is the planet's received XUV flux, $V_{pot} = GM/R$ is the gravitational potential magnitude at the base of the escaping region, and ϵ is an efficiency factor. XUV-driven loss is predicted to be fast on young planets around active stars: For $\epsilon = 0.1$, $F_{XUV} = 10^{-3}$ times the bolometric flux, and other parameters appropriate to early Earth, $\phi_E = 3.8 \times 10^{-10}$ kg m^{-2} s^{-1}, imply loss of an entire ocean's worth of H ($2 \times 7.6 \times 10^{22}$ mol) in only 25 My.

XUV-driven hydrodynamic escape is regarded as one of the most important escape mechanisms for H_2 from low-mass planets. Indeed, the 1.5–2.0 $R_\oplus$ radius gap (Fulton et al. 2017, Van Eylen et al. 2018) was predicted theoretically a few years before it was observed in models that invoked this escape mechanism (Lopez & Fortney 2013, Owen & Wu 2013). Over the last few years, however, it has become clear that many exoplanets may also lose large amounts of H due to a related process that has come to be known as core-powered mass loss[1] (Ikoma & Hori 2012, Ginzburg et al. 2018, Gupta & Schlichting 2019). In brief, core-powered mass loss is hydrodynamic escape that is driven by thermal energy from the planet's troposphere and deeper atmospheric regions, rather than from high-energy stellar photons absorbed in the thermosphere.

Both core-powered mass loss and XUV-driven escape may be important escape mechanisms for H from low-mass planets. However, there are important differences in the timescales on which they operate. For most host star types, XUV fluxes decline rapidly on a timescale of ~100 My or less after formation, whereas core-powered mass loss is believed to act on longer timescales of ~1 Gy (Lopez & Fortney 2013, Gupta & Schlichting 2019). Recently, an analysis of the Gaia–Kepler stellar properties catalog found significant differences in sub-Neptune versus rocky planet populations between systems with an age cutoff of 1 Gy, suggesting that the role of core-powered mass loss is significant (Berger et al. 2020). However, further analysis is required to definitively determine the key loss mechanism responsible for converting sub-Neptunes into rocky planets.

H loss can still occur even after H_2 is no longer the dominant species in a planet's atmosphere. In these circumstances, the bottleneck in loss usually becomes the rate at which H-bearing species such as H_2O or CH_4 can diffuse through the homopause in the upper atmosphere, as determined by the formula

$$\Phi_1 = b x_1 (H_{s,2}^{-1} - H_{s,1}^{-1}). \quad 3.$$

Here, Φ_1, x_1, and $H_{s,1}$ are the molecular flux, molar concentration, and scale height of the H-bearing minor species; $H_{s,2}$ is the scale height of the background atmosphere; and b is a binary diffusion coefficient (Hunten et al. 1987). This regime is called diffusion-limited escape.

Once H-bearing species reach the upper atmosphere, they are usually photolyzed rapidly, releasing H that then escapes to space. In some cases, the flux of the H-bearing species from the surface depends on chemical or even biological factors (e.g., CH_4 on the early Earth; Catling et al. 2001). However, the most important carrier of H on H_2-poor planets is usually H_2O, which is readily cold-trapped in the lowest regions of the atmosphere when a planet's equilibrium temperature is below the runaway greenhouse limit (Section 1.3). Cold-trapping of H_2O will protect against H loss, as long as the planet's inventory of noncondensing gases such as N_2 is sufficient (Wordsworth & Pierrehumbert 2013b). When cold-trapping fails, continued H loss can dramatically alter a rocky planet's chemistry over time, as we discuss further in Section 3.

Bolometric flux: total flux integrated over all wavelengths

Homopause: level in the atmosphere at which eddy diffusion equals molecular diffusion; above the homopause, the atmosphere is not well mixed and gas species begin to separate according to their masses

2.3. Loss of Volatiles to Space: Heavier Species

Elements heavier than H are harder to lose to space on terrestrial planets, which is fortunate for us, because it permits the survival of life on Earth. However, there are still many processes that

[1] In this context, "core" refers to the combined rocky and iron-rich portions of the planet.

contribute to heavy-element loss. The first is conceptually straightforward: These elements can simply be dragged along with the escaping H_2 during hydrodynamic escape. Indeed, in a well-mixed gas undergoing rapid escape, all elements will be lost in equal proportions. However, for moderate escape rates, escaping gases have time to diffusively separate, causing the heavier atoms or molecules to escape less rapidly. Below a certain critical escape flux, the loss of the heavier species is predicted to shut down entirely (Hunten et al. 1987).

The general equations for diffusion in a mixture of gases (Chapman & Cowling 1970) allow equations for hydrodynamic drag to be derived from first principles (Zahnle et al. 1990, Wordsworth et al. 2018). This conveniently allows the critical mass flux ϕ_c required to initiate drag of a heavy species along with a light species to be derived directly. One can show that this mass flux is simply $\phi_c = m_1\Phi_1$, with Φ_1 defined in Equation 3. Above the critical mass flux, the escape rate of the heavier species 2 is approximately

$$\Phi_2 \approx \begin{cases} 0 & : \phi < \phi_c \\ \left[x_2\phi + x_1x_2(m_1 - m_2)b/H_{s,1}\right]/\overline{m} & : \phi \geq \phi_c \end{cases}, \quad 4.$$

where $\overline{m} = m_1x_1 + m_2x_2$ is the mean molecular/atomic mass of the flow. Equation 4 is exact in the limit of subsonic, isothermal flow, and it is reasonably accurate in more general situations (Zahnle et al. 1990). It shows that both the mass difference between the two species and the scale height of the lightest species are important for determining the critical mass flux. A complementary expression for the escape rate of the lighter species can also be derived that reduces to Equation 3 when $\phi < \phi_c$.

Hydrodynamic drag matters for exoplanets because it influences the composition of a rocky planet's atmosphere after its primordial H_2 envelope has been lost to space (e.g., Malsky & Rogers 2020). Because the degree of heavy-element fractionation depends strongly on the rate of H_2 loss through time, atmospheric characterization may provide an additional way to distinguish among various loss mechanisms. Even direct measurements of isotope fractionation may be feasible in the future: It has been suggested that high-resolution ground-based or *JWST* transit observations could be used to detect highly deuterium-enriched water on rocky exoplanets such as Proxima Cen b or TRAPPIST-1 b (Lincowski et al. 2019, Mollière & Snellen 2019; see also Section 7).

Once most H_2 is lost to space, atmospheres become far more resistant to hydrodynamic escape, because the higher molecular mass increases the temperature required to achieve a given value of λ. For example, to achieve $\lambda = 10$ on an Earth-like planet with an O-dominated upper atmosphere given 1.3 $R_\oplus$, $T \sim 9{,}300$ K would be required. Whether or not such high temperatures can be reached depends on radiative and conductive effects in the thermosphere. Some gases (particularly CO_2) are predicted to cool the thermosphere effectively (Lichtenegger et al. 2010), although even CO_2 may be lost hydrodynamically from small, hot planets (Tian et al. 2009). Uncertainties in the nonlocal thermal equilibrium conditions (Lopez-Puertas & Taylor 2001) in the upper atmosphere currently limit our understanding of this regime.

On smaller planets and moons, the weaker gravity means that loss of heavy species like H_2O to space can occur much more readily (Arnscheidt et al. 2019). Finally, at extremely high temperatures, the definition of "volatile" shifts from species such as N_2 and CO_2 to Na, SiO, and Mg. Escape of these species to space is expected on extremely hot rocky planets and could explain the asymmetric transit profiles of some Kepler planet candidates (Rappaport et al. 2012, Kang et al. 2021).

An additional class of heavy-species escape processes exist that are nonthermal and hence not dependent on extreme heating of the thermosphere. Some nonthermal escape is still powered by stellar radiation. For example, photochemical escape occurs when photons break apart molecules

or ions with sufficient excess energy that some of the products move fast enough to escape to space, in reactions such as

$$O_2^+ + e^- \rightarrow O + O. \quad 5.$$

Pickup ion: a neutral species from a planet's upper atmosphere that becomes ionized and picked up by the local magnetic field

Other nonthermal loss processes involve interaction with the stellar wind. Examples of important processes in the Solar System include pickup ion escape and sputtering (Lammer et al. 2008). The importance of both these effects depends strongly on the properties of the planet's magnetic field. It is sometimes stated that a magnetic field is required to protect a planet from atmospheric erosion, but this is a misconception: The terrestrial planet with the thickest atmosphere in the Solar System (Venus) has no intrinsic magnetic field, and some simulations in fact predict an increase in escape rates as the dipole magnetic moment of terrestrial-type planets is increased (Gunell et al. 2018).

Complex three-dimensional (3D) models of nonthermal heavy-species escape have now been applied to various exoplanets, including the planets of the TRAPPIST-1 system (e.g., Garcia-Sage et al. 2017, Dong et al. 2018). The results of these models have suggested that high loss rates are possible from these planets, up to tens of bars of heavy species per gigayear. However, many uncertainties remain in these estimates, because of unknowns in planetary magnetic fields, atmospheric composition, and the efficiency of loss processes.

Systematic differences in escape with host star type are somewhat easier to assess. Much research to date has focused on the differences between G-stars like the Sun and M-stars, because of the observational opportunities for planets around M-stars discussed in Section 1. Three differences are particularly important. First, as noted in Section 2.1, M-dwarfs undergo a long pre–main sequence phase of elevated luminosity (up to several 100 My for stars like TRAPPIST-1; Baraffe et al. 2015). Second, many M-dwarfs emit considerably more XUV radiation over their lifetimes than G-dwarfs do, as a result of enhanced starspot activity and associated coronal heating (France et al. 2016, McDonald et al. 2019). Third, coronal mass ejection from M-dwarfs has been predicted to be significantly greater, although observational constraints on this prediction remain limited (Crosley & Osten 2018, Odert et al. 2020).

These differences all imply enhanced atmospheric removal in M-dwarf systems. The high pre–main sequence luminosity will push many young rocky planets that obtain H_2O during formation into a runaway greenhouse state, where their upper atmospheres remain dominated by water vapor for long time periods (**Figure 5**). This H_2O is readily photolyzed, and the high M-dwarf XUV fluxes can then power the escape of many Earth oceans' worth of water to space, desiccating the planet (Ramirez & Kaltenegger 2014, Luger & Barnes 2015, Tian & Ida 2015, Bolmont et al. 2017). Because hydrodynamic drag preferentially removes H, this loss has important implications for atmospheric chemistry, as we discuss further in Section 3.

A final major class of loss processes includes atmospheric blowoff by meteorite impacts and large protoplanet collisions during formation. Meteorites can deliver volatiles, but the kinetic energy they supply on impact can also be a significant driver of atmospheric loss (Melosh & Vickery 1989). This loss process is still incompletely understood, but it may have played a major role in Mars's atmospheric loss (Brain & Jakosky 1998) and could also explain why Titan today has a thick N_2 atmosphere while similar outer Solar System moons like Ganymede do not (Zahnle et al. 1992). Smaller impactors may have a particularly important role in determining the differences in the noble-gas inventories of Earth and Venus (Schlichting et al. 2015). However, few constraints on impactor fluxes to exoplanets over time currently exist.

Given all the uncertainties, empirical modeling of escape processes on rocky exoplanets is a compelling complementary approach. One example of such an approach is the cosmic shoreline, proposed by Zahnle & Catling (2017). These authors noted that the divide between airless bodies

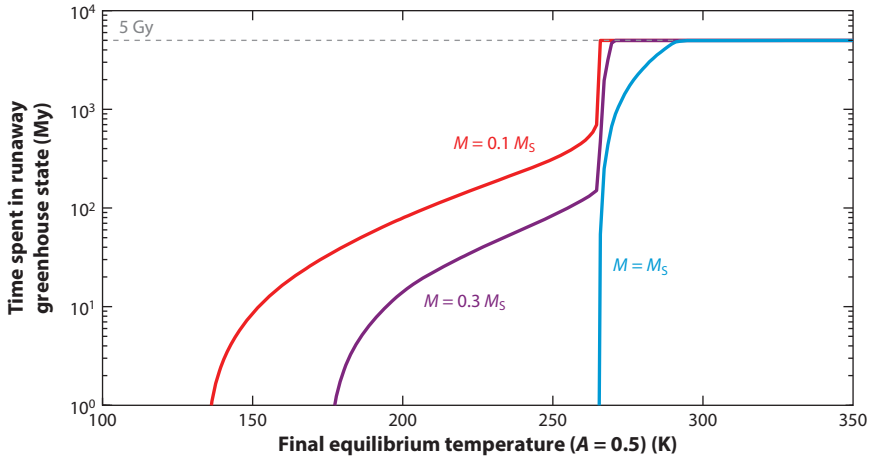

Figure 5

Total time spent in a runaway greenhouse state as a function of final equilibrium temperature, for rocky planets after 5 Gy of evolution. The extended pre–main sequence stage of low-mass stars causes planets that form around them to remain in a runaway greenhouse phase for up to several hundred megayears, leading to extensive water loss to space. Figure adapted from Luger & Barnes (2015).

and those with atmospheres in the Solar System follows a line $F \propto v_{esc}^4$, where F is the present-day bolometric solar flux and v_{esc} is the escape velocity for the body in question. Interestingly, the prediction from XUV-driven escape, which instead yields $F \propto v_{esc}^3$, conflicts with this empirical result. Data on the presence or absence of atmospheres for a wide range of exoplanets will be crucial for testing the generality of such scaling laws in the future (Section 7).

With future advances in instrumentation, it will become possible to test theories of escape directly. Lyman-α observations have already been used successfully to detect escaping H around gas-rich planets (Ehrenreich et al. 2015) and have been attempted for rocky planets, though only upper limits have been obtained so far (Kislyakova et al. 2019, Waalkes et al. 2019). Detecting escape of heavier elements is another possibility, particularly the metastable He absorption triplet, which is accessible with ground-based telescopes (Nortmann et al. 2018, Oklopčić & Hirata 2018). Escaping ionized metals may also be detectable (García Muñoz et al. 2021), as well as auroral emissions from species such as O (Luger et al. 2017).

3. ATMOSPHERIC CHEMISTRY

As noted above, the extreme diversity of rocky planet atmospheres relative to solar composition is an outcome of delivery and loss to space, internal chemistry, and exchange with the interior. In this section, we discuss atmospheric chemistry and lay the groundwork for discussing interior exchange (which is itself strongly dependent on chemistry).

3.1. Redox and Equilibrium Chemistry

To classify atmospheric composition in a systematic way, it is useful to invoke broad chemical principles. For rocky planets, the most important of these by far is redox. The redox state of a system can be defined by comparing the total quantity of atoms like H or Fe, which readily donate electrons (reducing species), with that of atoms like O, which readily accept electrons (oxidizing species). In a planetary context, H_2- and CH_4-rich atmospheres such as Titan's are classified

as highly reduced; CO_2- or N_2-dominated atmospheres with trace H_2 are weakly reduced; and atmospheres with an excess of O_2 relative to reducing species, such as modern Earth's, are oxidized (Kasting et al. 1979, Yung & DeMore 1999). Redox is closely tied to the topics of habitability and biogenesis, because reducing chemistry is necessary for prebiotic compounds like HCN to form in a planet's atmosphere (Ferris et al. 1978, Kasting & Brown 1998).

Bulk silicate earth (BSE): the bulk chemical composition of Earth, including the crust and mantle but omitting the core

Seen through the lens of redox, H loss to space becomes a net oxidation of the planet. The tendency of many rocky planets to oxidize can be viewed as a rather generic outcome of gravitational differentiation given the galactic abundance of elements, because H is lost to space and Fe sinks to the core, leaving an increased relative proportion of elements like O, C, and N on the surface and in the atmosphere (Zahnle et al. 2013, Wordsworth et al. 2018). Therefore, it is reasonable to expect that the oxidation state of rocky exoplanet atmospheres will be correlated with their total amount of H loss. This oxidation can potentially continue to extreme levels: Modeling suggests that in the absence of surface exchange, H loss from H_2O photolysis could lead to atmospheric O_2 buildup on a planet without any biosphere (Wordsworth & Pierrehumbert 2014, Luger & Barnes 2015). However, interaction with the surface and interior is an important additional process, as we discuss further in Section 4.

When an atmosphere's bulk elemental composition is known, equilibrium chemistry is the starting point for understanding which molecular species will be present. In pure equilibrium, atmospheric composition can be determined via minimization of Gibbs free energy and is solely a function of elemental abundance, temperature, and pressure. At high temperatures, atmospheres are expected to be close to an equilibrium state, although disequilibrium processes may dominate on cooler planets, as we discuss in the next subsection.

Equilibrium chemistry calculations and experiments for planets with temperatures in the range of 500 to 3,500 K predict a variety of possible atmospheric compositions, depending on temperature, pressure, and elemental abundance (Schaefer & Fegley 2009, Miguel et al. 2011, Schaefer et al. 2012, Thompson et al. 2021). Under the reducing H-rich conditions expected for the most primitive atmospheres, H_2, CO, and CH_4 are expected to dominate. When H, C, N, and S species are present but H is no longer a dominant species [e.g., for bulk silicate Earth (BSE) composition], H_2O, CO_2, SO_2, and Na are key atmospheric species (**Figure 6**). Finally, for highly evolved atmospheres from which all H, C, N, and S have escaped, Na, O_2, O, SiO, and Fe dominate atmospheric composition in the temperature range of 2,000 to 3,500 K.[2] These last results are relevant to several highly irradiated rocky exoplanets with $T_{eq} > 500$ K (**Table 1**).

3.2. Photochemistry and Other Disequilibrium Processes

Many rocky planets are cool enough for disequilibrium chemistry to play a major role in their atmospheric composition. On Earth, a key driver of chemical disequilibrium is life. Even on lifeless planets, however, disequilibrium is caused by a host of processes, including volcanism, lightning, meteorite impacts, stellar coronal mass ejection events, and, most importantly, photochemistry driven by stellar UV radiation (Airapetian et al. 2016, Ardaseva et al. 2017, Zahnle et al. 2020).

Photochemical effects are most important in the upper atmosphere, where stellar UV radiation is absorbed. On gas giants, descending air parcels always reach a depth where thermochemistry drives them to local equilibrium, but for rocky planets, thermochemistry is important only if temperatures in the lowest part of the atmosphere are high enough. Venus is the only rocky planet in the Solar System in this regime, but it may apply to many nearby rocky exoplanets. The shutdown

[2]These results assume that Na escapes less readily to space than do C, N, and S. In reality, it may also escape efficiently once atmospheric temperatures are high enough.

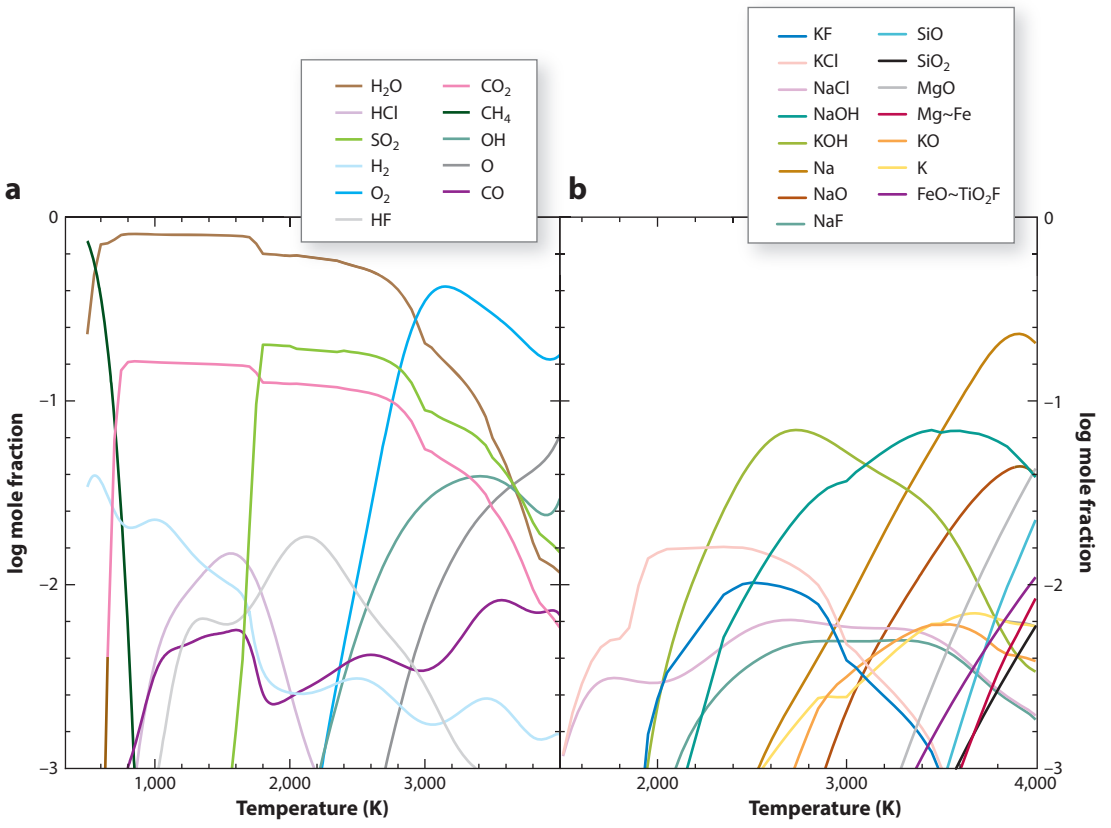

Figure 6

Hypothetical composition of a moderately oxidized exoplanet atmosphere assuming thermochemical equilibrium, bulk silicate earth (BSE) elemental abundances, and pressure of 100 bar. (*a*) More volatile species. (*b*) More refractory species. Results are shown as a function of temperature. Figure adapted from Schaefer et al. (2012).

of the drive to thermochemical equilibrium on planets with thin atmospheres could provide a way to probe exoplanet surface pressure indirectly in the future (Yu et al. 2021), although, as we discuss in the next section, interaction with the planet's interior can rarely be ignored.

Many photochemical modeling studies of rocky exoplanet atmospheres have focused on planets similar to Earth, although there is a steady trend toward more generalized models and conclusions. The problem of biosignature definition around different star types (particularly M-dwarfs) fueled several early studies (e.g., Selsis et al. 2002; Segura et al. 2003, 2007) and remains a key topic of interest. Other modeling studies have addressed a wide range of topics, including differences between oxic and anoxic atmospheres (Hu & Seager 2014), evolution of C- and S-bearing species (Hu et al. 2013, Hu & Seager 2014), the formation of prebiotic compounds such as HCN (Rimmer & Rugheimer 2019), and 3D coupling between chemistry and climate (e.g., Chen et al. 2019, Gómez-Leal et al. 2019).

One of the most important differences for photochemistry around stars like the Sun versus lower-mass stars lies in the UV portion of their spectrum (Rugheimer et al. 2015). Specifically, while K- and M-dwarfs emit a higher fraction of their luminosity in the XUV and far ultraviolet (FUV) range, they emit a lower fraction of their luminosity as near ultraviolet (NUV) and

Far ultraviolet (FUV): electromagnetic radiation in the 122–200 nm wavelength range

Near ultraviolet (NUV): electromagnetic radiation in the 300–400 nm wavelength range

longer-wavelength radiation because of their cooler photospheric temperatures. This leads to systematic differences in the ways that atmospheric chemical processes are expected to play out. One example is the photodissociation of CO_2 by photons of wavelength $\lesssim$200 nm:

$$CO_2 + h\nu \rightarrow CO + O. \quad 6.$$

In this reaction, the liberated O can readily form O_2, but reconversion of CO and O back to CO_2 is inhibited by the slow rate of the spin-forbidden reaction $CO + O + M \rightarrow CO_2 + M$. As a result, catalytic cycles involving radical species such as OH are critical to determining the ratio of CO_2 to CO and O_2. However, the rate of OH production depends on photolysis of H_2O in many atmospheres. H_2O is more fragile than CO_2 and hence can be dissociated by longer-wavelength NUV radiation.

Tian et al. (2014) and Gao et al. (2015) suggested that because M-stars have smaller NUV-to-FUV flux ratios than G-stars, photolysis of H_2O and hence production of OH on Earth-like planets orbiting them would be limited, leading to enhanced atmospheric abundances of CO and O_2. However, these results were recently followed by new experimental measurements of the NUV H_2O photodissociation cross section (Ranjan et al. 2020) indicating lower O_2 buildup due to the reaction in Equation 6 in some cases. The results obtained by Ranjan et al. (2020) highlight the continued importance of performing laboratory measurements in tandem with theoretical modeling in planetary chemistry.

To aid photochemical modeling in the future, accurate estimates of X-ray and UV fluxes from host stars will be essential, and observational campaigns to develop comprehensive stellar UV databases (e.g., Shkolnik & Barman 2014, France et al. 2016) must continue. Future theoretical research must also pay greater attention to uncertainties in both absorption cross sections and reaction rates. Monte Carlo photochemical simulations (e.g., Hébrard et al. 2005) allow key sources of uncertainty to be isolated and could help identify the new laboratory experiments and ab initio rate calculations that are most needed in the future.

Radical: an atom, molecule, or ion with an unpaired valence electron that is typically highly reactive

Aerosol: general term for any solid or liquid particle (cloud, haze, or dust) suspended in a gas

3.3. Aerosol Formation: Cloud Condensation and Photochemical Hazes

Aerosol formation due to condensation and heterogeneous chemistry is an extremely important and complex process in rocky planet atmospheres. Atmospheric aerosols may form purely due to condensation (e.g., H_2O or CO_2 clouds) or due to a combination of radical chemistry and condensation (e.g., H_2SO_4 aerosols and organic hazes). Clouds and aerosols have a major impact on observables and on planetary climate, because their radiative impact per unit mass is typically far greater than for species in the gas phase. Cloud and haze layers have been identified in the atmospheres of several hot Jupiter and sub-Neptune exoplanets (Knutson et al. 2014, Kreidberg et al. 2014, Sing et al. 2016), and there is every reason to expect they will be equally important on rocky exoplanets.

Photochemical hazes are a particularly important class of aerosols that occur primarily in reducing atmospheres rich in hydrogenated C species such as CH_4. Photolysis of CH_4 produces radicals such as CH_3, which can combine to form longer chain species and eventually condense to create haze particles. Photochemical hydrocarbon hazes are observed on many outer Solar System bodies, including, most famously, Titan. They are also present in the atmospheres of Jupiter and Saturn, although at lower abundance, because reaction of CH_3 and other radicals with H_2 is effective at inhibiting the buildup of C_nH_n chain species (Yung & DeMore 1999). Once they form, it is common for haze particles to aggregate into fluffy fractal particles that have unique radiative and microphysical properties (Rannou et al. 2003). Photochemical hazes are also thought to have been present on the early Earth, before the rise of O_2 (Domagal-Goldman et al. 2008,

Zerkle et al. 2012), and they may play an important role in the climates and observable properties of many rocky exoplanets (Arney et al. 2017).

Peridotite: the dominant rock type in Earth's mantle, composed of a mixture of SiO_2, MgO, and FeO

The incorporation of other elements such as N and O into haze particles depends on their abundance and reactivity. The N_2 bond is notoriously hard to break, but it can be dissociated by XUV radiation and energetic particles in the upper atmosphere or lightning in the lower atmosphere (Yung & DeMore 1999, Rimmer & Rugheimer 2019). N atoms can rapidly react with a number of species, including hydrocarbon radicals to form the quintessential prebiotic feedstock molecule, HCN. O is a minor contributor to haze particles on the outer Solar System planets and satellites because of H_2O cold-trapping, but it is likely to be important on a number of rocky exoplanets. Broadly speaking, haze formation is disfavored in atmospheres with low C-to-O ratios (below ~0.6; Trainer et al. 2006), but some production can still occur even when O_2 is present (Ugelow et al. 2018), as any resident of a polluted city on Earth knows.

S-rich hazes can form under both reducing and oxidizing chemical conditions. Under reducing conditions, S haze particles may consist of elemental S (S_8) or organosulfates (DeWitt et al. 2010). Under oxidizing conditions, photolysis of SO_2 and/or combination with OH radicals followed by condensation in the presence of H_2O leads to H_2SO_4 aerosols. These aerosols can dramatically increase a planet's albedo even in an atmosphere with low H_2O and SO_2 abundance, as is the case on present-day Venus. Because H_2SO_4 particles slowly sediment and are highly soluble in liquid water, the presence of a long-lived high-albedo H_2SO_4 cloud deck is incompatible with surface liquid water (Loftus et al. 2019) and probably also with a thin, nonthermolyzing atmosphere (see also Section 4).

Current understanding of other possible aerosol types on rocky exoplanets is limited, but growing. For example, Mbarek & Kempton (2016) performed a general study of chemical equilibrium condensate species in rocky and sub-Neptune exoplanet atmospheres for various compositions and temperatures ranging from 350 to 3,000 K. They predicted a wide variety of cloud types, including exotic possibilities such as K_2SO_4, ZnO, and graphite. Laboratory aerosol experiments also play an essential role in testing theoretical calculations and exploring the range of possibilities for exoplanet atmospheres. For example, Hörst et al. (2018) performed cold plasma discharge experiments and found haze production that was more diverse and widespread than predicted by theory. He et al. (2020) expanded this investigation to S species in CO_2-rich atmospheres and found an important role for H_2S in production of complex S products. Future progress in this area will require detailed intercomparisons between laboratory results and numerical chemical kinetic models.

4. ATMOSPHERE–INTERIOR INTERACTION

By definition, rocky planet atmospheres constitute a small mass fraction of the planets they envelop. As a result, their compositions are often strongly dependent on exchange with the interior. In this section, we discuss atmosphere exchange with several types of interior expected to be common on rocky exoplanets.

4.1. Exchange with Magma Oceans

Put simply, a magma ocean is a region of a rocky mantle that has reached temperatures sufficient to melt it. Rock compositions vary in the Solar System (and will likely vary even more for exoplanets), but for a typical peridotitic composition, the low-pressure solidus temperature is around 1,400 K, while the liquidus is around 2,000 K (Hirschmann 2000). Between these temperatures, a well-mixed magma consists of a slurry-like mixture of solid and liquid phases. With the possible exception of Io, whose interior is heated by tidal interactions with Jupiter (Khurana et al. 2011), silicate magma oceans are not observed in the Solar System today. However, several lines

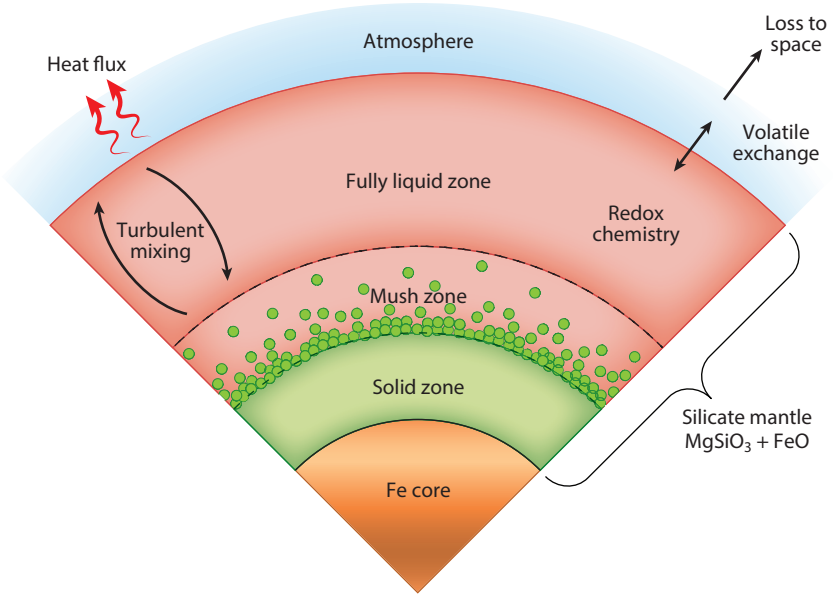

Figure 7

Schematic of a rocky planet interior with a magma ocean, indicating the solid–liquid transition with radius alongside key physical and chemical processes. Figure adapted in part from Lebrun et al. (2013).

of evidence indicate they played a crucial role in atmospheric evolution in the early Solar System, during and just after formation of the terrestrial planets (Elkins-Tanton 2012). Transient magma oceans are probably common on young rocky planets, and many hot rocky exoplanets may have permanently molten surfaces, particularly if they also possess thick atmospheres.

The mean depth of a magma ocean depends primarily on surface temperature. Convection in most magma oceans is expected to be intense enough for rapid exchange of volatiles with the atmosphere and an adiabatic vertical temperature structure to occur. The intersection of the magma adiabat with the solidus in pressure–temperature space is such that magma oceans should freeze from the bottom upward (Elkins-Tanton 2012, Lebrun et al. 2013). Importantly, this means that magma oceans should continue to efficiently exchange volatiles with the overlying atmosphere until they solidify at the surface (**Figure 7**).

In the absence of external heating, airless planets with magma oceans cool rapidly: Given a magma heat capacity of 1,200 J kg^{-1} K^{-1}, density of 3,000 kg m^{-3}, and flux to space of $F = \sigma T^4$ (where σ is the Stefan constant and T is temperature), the timescale to cool a 100-km-deep magma ocean from the liquidus temperature to the solidus is of order $\tau_{cool} \sim 15$ years. However, magma ocean cooling is dramatically slowed or even halted by the presence of an atmosphere, because of absorption of upwelling IR radiation (i.e., the greenhouse effect).

Atmospheric IR opacity depends on composition. Because H_2 is a particularly potent greenhouse gas at pressures above ~0.1 bar (Section 1.3), rocky planets that form with even thin H_2 envelopes will initially have completely molten surfaces (Hayashi et al. 1979, Chachan & Stevenson 2018). H_2O is also a strong greenhouse gas, but it condenses when a planet's equilibrium temperature is below the runaway greenhouse limit. This may have been important to the divergent evolution of Venus and Earth, because Earth's received solar flux was low enough to allow condensation of water after a few megayears, while Venus would have retained a steam

atmosphere until most of its H_2O was destroyed by photolysis followed by H loss to space (Hamano et al. 2013). This divergence based on received stellar flux may also be important for the atmospheric evolution of many exoplanets (Kane et al. 2019).

wt%: ratio of element mass to total mass, expressed as a percentage

Redox buffer: a collection of minerals that together define the chemical state of a silicate mantle region

Magma oceans affect atmospheric composition because atmospheric volatiles dissolve in them and sometimes interact with them chemically. The partitioning of gases into a magma depends strongly on its redox state (e.g., Gaillard et al. 2022). The most important determinant of redox in a silicate mantle is Fe, because of its abundance and ability to transition between the metallic Fe (Fe^0), Fe^{2+}, and Fe^{3+} states (Mg is also abundant in the mantle, but it is nearly always found in the +2 oxidation state). A high abundance of Fe^0 and Fe^{2+} corresponds to highly reducing conditions, while the Fe^{3+} oxidation state is abundant only in highly oxidizing conditions.

Fe segregation to a rocky planet's core during formation is never 100% efficient, as it depends on factors such as FeO equilibrium chemistry during core formation (Fischer et al. 2011). On the basis of modeling and analogy with the Solar System, mantle Fe contents of a few to 10 wt% or more for rocky exoplanets are expected. This translates to a vast chemical reservoir. As an example, if all the Fe in Earth's mantle (around 6 wt%; Javoy 1999) were in the form of Fe^{2+}, conversion to Fe^{3+} through the reaction $2FeO + O \rightarrow Fe_2O_3$ could consume the O equivalent to around 28 Earth oceans (2.2×10^{24} mol). This means that if a magma ocean is present on planets that are oxidizing through H_2O photolysis and H loss, it can absorb huge amounts of O before O_2 begins to build up in the atmosphere.

Geochemists usually express mantle redox state in terms of various mineral redox buffers. In terms of Fe, this translates to differing proportions of Fe^0, Fe^{2+}, and Fe^{3+}. Earth's upper mantle today is close to the quartz–fayalite–magnetite buffer, with $Fe^{3+}/Fe_{tot} \sim 0.03$ (where Fe_{tot} is the total Fe abundance of the mantle) (Armstrong et al. 2019). During Earth's formation, however, differentiation was ongoing and much more Fe^0 was present. The mantle was hence much more reducing, probably below the iron–wüstite (IW) buffer, with an Fe^{3+}/Fe_{tot} ratio of around 0.004 (Armstrong et al. 2019). Earth's increase in mantle oxidation over time may be due in part to early oxidation of the atmosphere via H loss. However, modern ^{2}H-to-H ratios in terrestrial seawater are quite close to the value for chondritic meteorites. This observation suggests that Earth's total loss of H from H_2O photolysis was relatively modest (e.g., Zahnle et al. 2020), probably because of effective cold-trapping of water in the lower atmosphere. Venus, in contrast, may have a highly oxidizing mantle closer to the magnetite–hematite (MH) buffer due to extensive early H loss, although more data on its surface geochemistry are needed (Fegley et al. 1997, Wordsworth 2016a).

Another process, Fe redox disproportionation, may also have played a role in mantle redox evolution on Earth (Armstrong et al. 2019) and is likely important on exoplanets. In this process, Fe in the 2+ oxidation state disproportionates to Fe^{3+} and Fe^0:

$$3Fe^{2+} \rightarrow Fe^0 + 2Fe^{3+}. \quad 7.$$

Because the density of Fe^0 is greater than that of mantle minerals, it sinks to the core. After core formation is complete, the end result is a more oxidized mantle. Redox disproportionation is yet another example of the deep connection between gravitational differentiation and chemical evolution on rocky planets. It is most efficient at high pressure, so planets of Earth mass and greater are expected to develop oxidized mantles more efficiently than smaller planets such as Mars (Deng et al. 2020).

Because the atmosphere and interior exchange volatiles rapidly when a magma ocean is present, the mantle redox state is a key determinant of atmospheric composition in this case. A reducing magma ocean near the IW buffer would outgas species like CO and H_2. Conversely, a planet with enough Fe^{3+} to place it above the MH buffer would be so oxidized that O_2 itself would become an important volatile outgassed to the atmosphere.

Mantle redox also determines the solubility of key volatile species such as C and N in magma. Under oxidizing conditions, CO_2 is the chemically favored form of dissolved C in magma oceans. The solubility of CO_2 in magma is low, which means that C-rich oxidized magma ocean planets are generally expected to have dense CO_2 atmospheres (e.g., Lebrun et al. 2013). However, in a reducing magma, C forms C–O and C–H species, Fe–carbonyl complexes, and even graphite, greatly increasing solubility and hence limiting the atmospheric CO_2 abundance (Grewal et al. 2020, Fischer et al. 2020). The behavior of N is similar: N_2 is quite insoluble in oxidized magmas, but it has greatly enhanced solubility under more reducing conditions (Libourel et al. 2003, Grewal et al. 2020). This redox dependence of interior sequestration implies that rocky planets with reducing mantles should have relatively C- and N-poor atmospheres, which may have important implications for future observations.

The theoretical understanding of magma ocean interaction with atmospheres on rocky exoplanets has evolved rapidly over the last decade. Several studies have now analyzed the changes in atmospheric composition resulting from exchange with magma oceans of different compositions, volatile abundances, and redox states (Lupu et al. 2014, Kite et al. 2016, Katyal et al. 2020, Lichtenberg et al. 2021). The development of models that can track the evolving redox chemistry of the atmosphere–magma ocean system as H is progressively lost to space (Schaefer et al. 2016, Wordsworth et al. 2018, Krissansen-Totton et al. 2021a) has also been an important step forward. Notably, these studies have demonstrated that while magma oceans are huge sinks for O liberated from water loss, there are still many situations where O_2-dominated atmospheres can appear abiotically, particularly on hot planets.

Testing the predictions of coupled atmosphere–magma ocean models observationally is an important future goal. While many processes contribute to atmospheric evolution, modeling suggests that the oxidation state of a planet's atmosphere should be correlated with the planet's radius, orbital distance, and host star type, with close-in planets around M-type stars particularly likely to have oxidized atmospheres. Theoretical predictions for the most accessible targets listed in **Table 1** are discussed further in Section 7.

4.2. Exchange with Water and Other Liquids

H_2O is cosmically abundant and central to the concept of habitability (Section 7), so water oceans are another important type of liquid surface to consider on low-mass exoplanets. Many theoretical studies on this topic have focused on rocky planets that have such high surface H_2O inventories that they no longer have any exposed land (waterworlds). Variability in H_2O delivery and loss (Section 2) means that such planets may be common, and initial modeling suggests that their atmospheres and climates should be dramatically different from Earth's.

The solubility of chemical species in H_2O varies widely. While nonpolar species such as N_2 and H_2 are relatively insoluble, others (CO_2, NH_3, SO_2) are readily dissolved (e.g., Pierrehumbert 2010b, Abbot et al. 2012). The solubility of CO_2 in particular decreases with temperature in the 300–400 K temperature range (Carroll et al. 1991). This can lead to destabilizing feedbacks, because more outgassing implies warmer surface temperatures that, in turn, cause still more outgassing (Wordsworth & Pierrehumbert 2013b, Kitzmann et al. 2015). Various proposals have been put forward to allow CO_2 levels to remain at the right level in the atmospheres of waterworlds to maintain habitable temperatures (Levi et al. 2017, Kite & Ford 2018, Ramirez & Levi 2018). However, for many volatile-rich planets, it is plausible that enough CO_2 could be acquired during formation to prevent the surface condensation of water to form oceans in the first place (Marounina & Rogers 2020). The question of waterworld habitability is discussed further in Section 7.

The solubility of other volatile species in water may provide opportunities to identify liquid water oceans on exoplanets. For example, Loftus et al. (2019) showed that the high solubility of oxidized S in water should limit atmospheric abundances of SO_2 and H_2SO_4 to undetectable levels on planets with even small surface oceans (although transient SO_2 can still be present as a result of volcanism; Kaltenegger & Sasselov 2009). Hu et al. (2021) recently proposed that a similar approach could be applied using NH_3 to identify water oceans on rocky planets with H_2-dominated atmospheres. However, N is soluble in the reducing magmas that are expected when H_2 is the dominant atmospheric gas, so it is unclear whether such observations could distinguish water oceans from magma ones.

Comparatively little research has been done on interior exchange involving other liquids. Photochemical haze formation (Section 3.3) can lead to formation of hydrocarbon lakes, as on Titan (Mitri et al. 2007), or mixtures of even more complex organics, as may have happened on the early Earth (Arney et al. 2017). On a planet with a moderately or strongly reducing atmosphere, thick layers of liquid hydrocarbons or more complex organics could build up on the surface over time in the absence of strong sinks. The implications of hydrocarbon oceans or other exotic possibilities for atmospheric observables have not yet been studied in any detail.

4.3. Solid Surface Exchange Processes

When planetary surfaces solidify, the rate of volatile exchange with the atmosphere changes dramatically. The internal mixing timescales of oceans (magma, water, or otherwise) are typically very fast compared with atmospheric loss and supply timescales, so equilibrium with the atmosphere can usually be assumed. In contrast, the mixing timescales of solid interiors are orders of magnitude slower (e.g., ~1 Gy for He in Earth's mantle; Coltice & Schmalzl 2006). Furthermore, there is still great uncertainty in how mantle convection and tectonics evolve on rocky planets through their lifetimes (Noack & Breuer 2014, Hawkesworth & Brown 2018). For all of these reasons, predicting solid surface exchange processes for exoplanets is a huge challenge.

Volcanic outgassing is the primary process by which volatiles are released from Earth's interior. The rate of volcanic outgassing depends on the rate of crustal production, which itself is a function of the tectonic regime of the planet. On a planet in a plate-tectonic regime, such as present-day Earth, volatile evolution models can be constructed that track the outgassing of species like H_2O over time using scaling parameters from convection theory (e.g., Schaefer & Sasselov 2015). Certain broad trends are predicted from such models. For example, many young planets with high mantle potential temperature should experience fast crustal growth and high rates of volcanic outgassing (Höning et al. 2019).

The scaling of tectonic regime with planet mass is less well understood. Early research suggested that plate tectonics becomes more likely as a planet's mass increases (Valencia et al. 2007), but this idea has since been contested. Subsequent studies have suggested that factors such as the presence or absence of H_2O (Korenaga 2010) or the planet's thermal history (Lenardic & Crowley 2012) may be more important than its mass. For planets in the stagnant-lid regime, outgassing rates are expected to decrease with increasing planet mass (Noack et al. 2017). Given the uncertainties about whether plate tectonics will occur, a wide range of possible outgassing rates should be expected.

What solid interiors provide to atmospheres via outgassing they can also take away, because atmospheric volatiles react chemically with planetary crusts. As with other chemical processes, the reaction rates are strong functions of temperature, but they also depend on the presence of solvents, particularly liquid H_2O. Carbonate formation is a classic example of a process that is thermodynamically favored at Earth-like temperatures but dependent on the presence of liquid

water to proceed at geologically important rates. In this process, Ca and Mg cations produced from the weathering of fresh igneous rocks react in seawater with bicarbonate ions:

$$Ca^{2+} + 2HCO_3^- \rightarrow CaCO_3 + CO_2 + H_2O, \quad 8.$$

removing net CO_2 from the atmosphere–ocean system in the process. On Earth today, the rate of carbonate formation is sufficient to completely remove CO_2 from the atmosphere–ocean system on a timescale of under a million years (Berner 2004). This does not happen because removal of CO_2 into carbonates is balanced by volcanic outgassing. A negative feedback, the carbonate–silicate cycle, is believed to keep volcanic outgassing and carbonate formation closely balanced on long timescales on Earth (Walker et al. 1981; see also Section 7).

Phyllosilicates: hydrated silicate minerals, including clays, micas, and serpentines, that form in parallel sheets of silicate bonded with water or hydroxyl (OH) groups

Numerous additional reactions between volatiles and crustal material are important for rocky planet atmospheric evolution. Phyllosilicate formation due to interaction of igneous rocks with water can constitute a significant H_2O sink to the crust and/or mantle over time. Serpentines are particularly interesting from an atmospheric standpoint, because reduced gases such as H_2 and CH_4 may be produced as a by-product of their formation, which can have many implications for chemistry and climate (Oze & Sharma 2005, Etiope et al. 2013, Wordsworth et al. 2017). Aqueous chemistry can also facilitate redox reactions, particularly the oxidation of Fe by UV radiation or atmospheric O_2 (Klein 2005, Hurowitz et al. 2010). This is particularly important for the question of when O_2 can be regarded as a biosignature on Earth-like exoplanets (Section 7).

For planets that do not possess surface liquid water, dry atmosphere–crust reactions can still be important if surface temperatures are high enough, as is the case on Venus in the Solar System today (Zolotov 2018). On rocky exoplanets with surface temperature in the range of 500 to 1,400 K, this class of reactions is also likely to be important, although our understanding of the range of possibilities is currently poor. For planets with solid compositions that have no analog in the Solar System (e.g., C-rich worlds), we currently have only a limited understanding of the range of possible tectonic regimes or atmosphere–interior interaction chemistries, although major differences from the Solar System planets appear plausible (Unterborn et al. 2014, Hakim et al. 2019). Again, more theoretical and laboratory analyses will be required to help constrain atmospheric evolution models in the future.

5. ATMOSPHERIC DYNAMICS AND CLIMATE

All planetary atmospheres are in a state of continuous motion as a result of differential heating and rotation. In contrast to gas giant planets, where heat fluxes from the interior can be important, atmospheric motion on the vast majority of rocky planets is driven by stellar radiation. Atmospheric dynamics determines wind speeds, which are potentially observable via high-resolution Doppler spectrometry, and heat transport from hot to cold regions of the surface, which leaves observable signatures in thermal phase curves (Section 6). It also influences atmospheric composition and cloud formation by determining the distribution of condensable species such as H_2O, which in turn affects a planet's potential habitability.

Atmospheric dynamics is studied theoretically via a range of tools, from pen-and-paper analytics to global circulation models (GCMs) that solve the fluid dynamical equations of a planet's atmosphere in three dimensions. Several studies have now systematically investigated how atmospheric dynamics is likely to change as a function of planet mass, rotation rate, stellar distance, atmospheric shortwave opacity, and other factors (e.g., Showman et al. 2013; Carone et al. 2014, 2015, 2016; Kaspi & Showman 2015; Read et al. 2018; Wang et al. 2018; Kang & Wordsworth 2019; Komacek et al. 2019; Auclair-Desrotour & Heng 2020). Broadly speaking, these studies have shown that the temperature variations across a rocky planet's surface increase with planetary

radius and rotation rate and decrease with atmospheric pressure. Wind speeds also vary greatly, with equatorial superrotation often occurring on planets with slow rotation rates or elevated visible wavelength atmospheric opacity.

Equatorial superrotation: dynamical regime where the angular momentum of the atmosphere is greater than that of the solid planet near the equator

Rossby wave: planetary-scale atmospheric wave that propagates westward at mid-latitudes on a rotating planet

Equatorial Kelvin wave: planetary-scale atmospheric wave that propagates eastward along the equator on a rotating planet

5.1. Atmospheric Circulation of Tidally Locked Planets

The atmospheric circulation of rocky planets around M-dwarf stars has received special theoretical attention over the last decade. Because M-dwarfs are dim compared with the Sun, planets around them that receive similar stellar fluxes to Earth are in close orbits. For example, Proxima Centuri b, which receives 65% of the flux of Earth, has a semimajor axis of 0.0485 AU and a year length of only 11.2 days (Anglada-Escudé et al. 2016). For such small star–planet separations, tidal effects are extremely important. Therefore, many M-dwarf rocky planets are predicted to have low orbital obliquities and tidally resonant orbits (Heller et al. 2011), although on some planets asynchrony may be maintained by atmospheric thermal tides (Leconte et al. 2015). The most extreme case of tidal interaction is a one-to-one resonance, or tidal locking. A planet in this configuration has permanent day- and nightsides, which profoundly affect its atmospheric circulation and climate.

Theory and modeling predict that a planet with permanent day- and nightsides will develop strong convergence and upwelling around the substellar point, horizontal transport from dayside to nightside, and a return flow to the dayside near the surface, in a kind of global convection cell (**Figure 8**). Planetary rotation breaks the radial symmetry of this flow along the substellar/antistellar axis, which forces the development of Rossby and equatorial Kelvin waves (Merlis & Schneider 2010, Showman & Polvani 2010). The resulting flow pattern then drives angular momentum toward the equator, leading to equatorial superrotation in many cases (Merlis & Schneider 2010, Showman & Polvani 2011). On planets with thick atmospheres, the interaction of the deep and upper atmospheres makes predicting equilibrated superrotating flows a significant

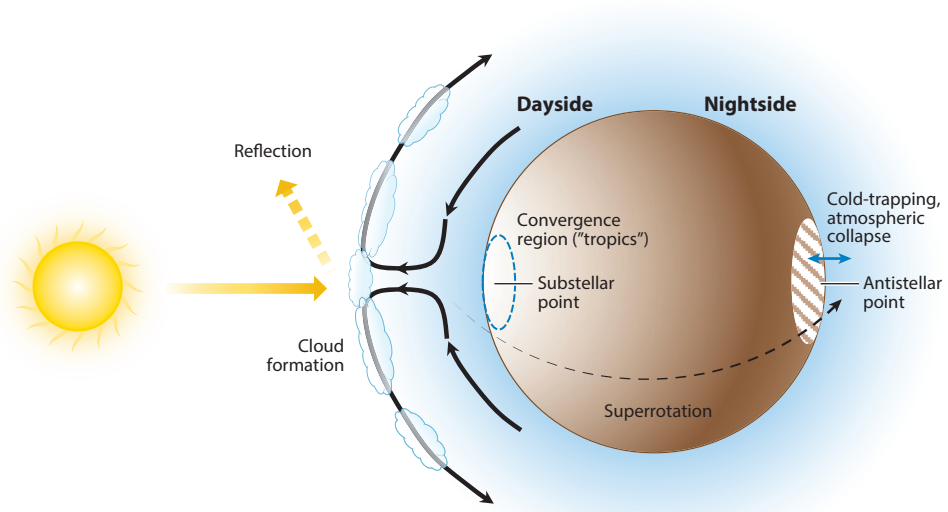

Figure 8

Key dynamical and climate processes in the atmosphere of a tidally locked rocky exoplanet. The hydrological cycle depends on the total H_2O inventory and other factors. Cloud coverage and surface inventories are shown here for a planet with low total H_2O compared with Earth.

challenge (Carone et al. 2020, Wang & Wordsworth 2020), but for rocky exoplanets with thinner atmospheres, flow equilibration times are much shorter and model predictions are in principle more reliable. Direct measurement of the wind speed in a rocky exoplanet atmosphere remains a key future observational goal (Section 7.1).

The horizontal heat transport by atmospheres on tidally locked planets is particularly important because of its effect on thermal phase curves and volatile transport. On fast-rotating planets, the presence of eddies and turbulence makes this heat transport challenging to predict, although scaling theories have been developed (Komacek et al. 2019). On slower rotators, the weak temperature gradient approximation can be made, greatly aiding analyses (Merlis & Schneider 2010, Pierrehumbert 2010a, Wordsworth 2015, Koll & Abbot 2016). An atmosphere in a weak temperature gradient regime can be treated as isothermal above the planetary boundary layer, so the interhemispheric heat transport problem boils down to determining the enthalpy fluxes (sensible, radiative, and latent) between the surface and atmosphere in each hemisphere (Wordsworth 2015, Koll & Abbot 2016, Auclair-Desrotour & Heng 2020). Both 3D modeling and theory predict that nightside warming strongly increases with both the pressure and the IR opacity of the atmosphere. For condensable species like CO_2, the pressure dependence can lead to a runaway process called atmospheric collapse (Section 5.2).

Atmospheric heat transport is one of the few processes that has already been tested observationally on a rocky exoplanet. Using the Infrared Array Camera (IRAC) on *Spitzer*, Kreidberg et al. (2019) performed thermal phase curve observations of the hot rocky exoplanet LHS 3844 b (see also Section 6). They found a symmetric phase curve and a high dayside flux, implying inefficient dayside-to-nightside heat transport and hence a thin atmosphere. Via a detailed comparison with theory, the authors ruled out the presence of an atmosphere with surface pressure above 10 bar. Thermal phase curve analysis is expected to be a key tool for atmospheric characterization of rocky exoplanets in the future, particularly when combined with spectral analysis (Selsis et al. 2011).

5.2. Cold-Trapping, Atmospheric Collapse, and Ice–Albedo Feedbacks

Condensation is fundamental to determining the atmospheric composition of rocky planets. When horizontal heat transport is ineffective, some regions of the surface can become much, much colder than the planet's equilibrium temperature. These regions then act as cold traps for volatile species. If the cold-trap temperature T_c is known, predicting the atmospheric abundance of a cold-trapped species is simple: In the absence of any additional sinks or sources in the atmosphere, it is uniquely determined by the saturation vapor pressure $p_{sat}(T_c)$ (e.g., Leconte et al. 2013, Ding & Wordsworth 2020).

On rocky bodies in the Solar System, permanently shadowed regions can be incredibly effective cold traps. Even Mercury, which receives almost seven times the solar flux of Earth, exhibits evidence of water ice and organic deposits in polar craters that are permanently shielded from sunlight (Neumann et al. 2013). GCM simulations predict that for a tidally locked exoplanet with Earth's atmospheric composition, water would rapidly become trapped as ice on the nightside (Leconte et al. 2013). However, when dayside tropopause temperatures are cold enough, an "oasis" regime can result where some water remains trapped as liquid on the planet's dayside (Ding & Wordsworth 2020).

Atmospheric collapse is the extreme limit of volatile cold-trapping when the main component of the atmosphere is the species that condenses. Atmospheric collapse may sound dramatic, but it is actually common in our Solar System: Mars, Triton, and Pluto are all in collapsed atmosphere regimes. Once collapse starts, it is usually a runaway process, because thinner atmospheres transport heat and warm the surface less effectively, making cold-trap regions even colder. For

gases like H_2O, collapse is the direct inverse of the runaway greenhouse process mentioned in Section 1.3.

In the 1990s, climate researchers initially thought atmospheric collapse might be fatal to the habitability of planets around M-stars, so it was one of the first exoplanet questions to be studied using a 3D climate model (Joshi et al. 1997, Joshi 2003). Recent GCM simulations with real-gas radiative transfer predict that the collapse pressure for pure CO_2 is a function of stellar flux and planet mass, with values from around 0.1 bar to 10 bar in the ranges of 1–10 M_E and 500–4,000 W m^{-2} (Wordsworth 2015, Turbet et al. 2016). Very hot rocky exoplanets for which Na, SiO, and Mg are the main volatile species are also expected to be in collapse regimes. Simplified circulation modeling suggests that flows on such planets will be supersonic from dayside to nightside, analogous to the SO_2 circulation regime on Io (Castan & Menou 2011, Kang et al. 2021).

When volatiles condense across wide regions of a planet's surface, they can alter albedo and hence surface temperature, causing climate feedbacks. Ice–albedo feedbacks involving H_2O were responsible for the Snowball glaciations that occurred in Earth's past (Hoffman et al. 1998). On exoplanets, the frequency of Snowball transitions likely depends on factors such as the mean rate of volcanic outgassing and the internal variability of the carbon cycle (Haqq-Misra et al. 2016, Wordsworth 2021). However, around M-dwarfs, the redder stellar spectrum weakens the feedback by decreasing ice albedo (Joshi & Haberle 2012, Shields et al. 2013) and tidal locking may inhibit Snowball bifurcations entirely (Checlair et al. 2017, 2019).

5.3. Clouds and Climate

Clouds are important because they affect observables and climate. They are also a huge challenge to model. Once clouds condense, they can scatter and/or absorb both incoming visible and outgoing IR radiation, depending on their composition and size distribution. Species that absorb in the UV, visible, or near IR (NIR), such as photochemical hazes and ozone (O_3), can cause strong temperature inversions in the atmosphere and an antigreenhouse effect that lowers surface temperatures (McKay et al. 1991). However, many condensates, including H_2O and CO_2 clouds, mainly scatter visible radiation. The net climate effect of these species then comes down to a competition between visible scattering and IR extinction effects, which leads to variations in the sign of radiative forcing with cloud altitude (Pierrehumbert 2010b).

Multiple studies have now modeled radiatively active clouds on rocky exoplanets using GCMs (e.g., Wordsworth et al. 2011, Yang et al. 2013, Kopparapu et al. 2016, Turbet et al. 2016, Wolf 2017, Sergeev et al. 2020, Lefèvre et al. 2021). Among other things, these studies have shown that CO_2 clouds can cause warming on cool planets with thick CO_2 atmospheres via IR scattering, supporting earlier predictions from one-dimensional models (Forget & Pierrehumbert 1997). Beginning with Yang et al. (2013), they have also suggested that on slowly rotating planets, concentrated water clouds can cause enhanced reflection of starlight around the substellar point. This could help planets around M-stars maintain surface liquid water at higher incident stellar fluxes than planets around G-stars.

In all cases, the overall magnitude of cloud effects depends on details of cloud microphysics and convection, which are usually poorly constrained. First-principles studies that focus on the behavior of convection (e.g., Ding & Pierrehumbert 2016, 2018) or cloud and precipitation microphysics (e.g., Zsom et al. 2012, Gao & Benneke 2018, Loftus & Wordsworth 2021) under a wide variety of different regimes are important for future progress in this area. Finally, and perhaps most importantly, clouds matter to exoplanet observations, most often because they obscure the detection of other spectral features. Komacek et al. (2020) and Suissa et al. (2020) studied the effects of clouds on *JWST* transmission spectroscopy and concluded that detection of water vapor

Table 2 Summary of transmission spectroscopy results for rocky planets with M-dwarf host stars

Planet	Result	Facility	Reference(s)
GJ 1132 b	Solar composition ruled out (16.3σ)	*HST*/WFC3	Libby-Roberts et al. (2021)
LHS 1140 b	Marginal evidence for H_2O (2.7σ); may be due to stellar contamination	*HST*/WFC3, Magellan/IMACS, LDSS3C	Edwards et al. (2021), Diamond-Lowe et al. (2020a)
LHS 3844 b	Solar composition ruled out (5.2σ)	Magellan/LDSS3C	Diamond-Lowe et al. (2020b)
TRAPPIST-1 b	Solar composition ruled out (7σ)	*HST*/WFC3	de Wit et al. (2016)
TRAPPIST-1 c	Solar composition ruled out (7σ)	*HST*/WFC3	de Wit et al. (2016)
TRAPPIST-1 d	Solar composition ruled out (8σ)	*HST*/WFC3	de Wit et al. (2018)
TRAPPIST-1 e	Solar composition ruled out (6σ)	*HST*/WFC3	de Wit et al. (2018)
TRAPPIST-1 f	Solar composition ruled out (4σ)	*HST*/WFC3	de Wit et al. (2018)
TRAPPIST-1 g	Solar composition disfavored (2σ)	*HST*/WFC3	de Wit et al. (2018)

will be extremely difficult on water-rich Earth-like planets if spectral features are truncated by a cloud deck. The challenge posed to future observations by clouds is discussed further in Section 6.

6. CURRENT OBSERVATIONAL CONSTRAINTS

As discussed in Section 1, observations of rocky planet atmospheres are rapidly developing as new systems are discovered and telescope capabilities grow. In this section, we provide a snapshot of the current state of knowledge, and in Section 7, we discuss prospects for future observations.

Hubble Space Telescope (*HST*) and *Spitzer* have been the workhorse observing facilities for rocky planet characterization over the last decade. These space telescopes provide precise, repeatable measurements that are free of contamination from the Earth's atmosphere (e.g., Kreidberg et al. 2014, Ingalls et al. 2016). The Wide Field Camera 3 (WFC3) instrument on *HST* is capable of low-resolution spectroscopy ($R \sim 100$) in the NIR between 1.1 and 1.7 μm, and *Spitzer*/IRAC provides photometry in two broad band passes centered at 3.6 and 4.5 μm (Fazio et al. 2004, Kimble et al. 2008). Ground-based telescopes have also been used to measured a handful of transmission spectra at optical wavelengths (**Table 2**). Direct imaging instrumentation is not yet sensitive to rocky planets, so all observational constraints so far are for transiting systems.

Transmission spectra are currently the most common type of observation. These data are sensitive to molecular and atomic absorption as well as to the presence of clouds. For a smaller sample of planets, thermal emission and reflected light observations are also available. To date, rocky planet atmosphere characterization has focused on only 10 of the most observationally accessible systems. Nearly all of these are transiting planets orbiting nearby M-dwarfs. These small stars are advantageous targets because they are (*a*) more numerous than Sun-like stars, leading to a larger sample; (*b*) smaller in radius, which increases the signal-to-noise of the planet's atmospheric features; and (*c*) cooler, leading to Earth-like temperatures closer to the star where planets are statistically more likely to transit. These advantages are colloquially known as the M-dwarf opportunity. A few ultrashort-period planets around larger stars are also accessible (notably 55 Cancri e); we discuss these in Section 6.2.

6.1. Planets with M-Dwarf Host Stars

Transmission spectra have been measured for nine rocky planets with M-dwarf hosts: GJ 1132 b, LHS 1140 b, LHS 3844 b, and TRAPPIST-1 b–g. The measured spectra are generally featureless, that is, consistent with a constant transit depth over the observed wavelength. **Figure 9** shows representative spectra from *HST*/WFC3 for the two inner planets in the TRAPPIST-1 system

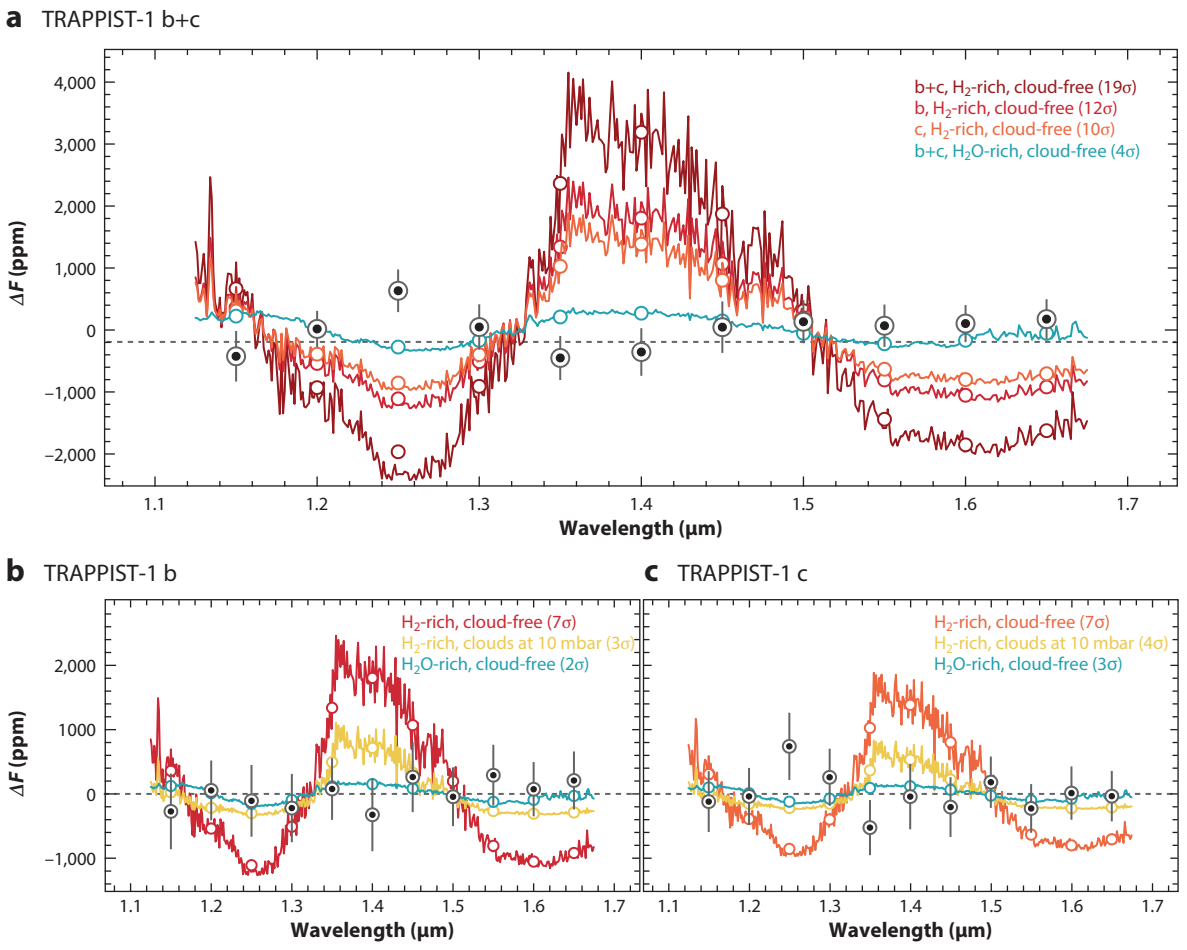

Figure 9

Transmission spectra (*black points*) for the planets TRAPPIST-1 b and c, measured with the *Hubble Space Telescope* Wide Field Camera 3 (from de Wit et al. 2016). (*a*) Combined spectra from both planets. (*b*,*c*) Each planet spectrum separately. The data are compared with theoretical model predictions for a range of atmospheric compositions (*colored lines*). A cloud-free, H-rich atmosphere is ruled out at 7σ confidence for both planets, but a high mean molecular weight composition of pure H_2O is marginally consistent with the observations. High-altitude clouds (below 10 mbar pressure) or the absence of an atmosphere could also produce a featureless spectrum.

(de Wit et al. 2016). These featureless spectra are precise enough to rule out cloud-free solar composition (i.e., H_2-dominated) atmospheres for all but two of the planets studied so far, with a range of significance from 4σ to 16σ (listed in **Table 2**). The spectrum of TRAPPIST-1 g has a lower signal-to-noise ratio but still disfavors a solar composition at 2σ confidence. In two cases, spectral features in an H_2-rich atmosphere were claimed for GJ 1132 b (Southworth et al. 2017, Swain et al. 2021), but subsequent research ruled out both detections (Diamond-Lowe et al. 2018, Libby-Roberts et al. 2021, Mugnai et al. 2021). A Lyman-α transit observation provided further evidence against an H_2-rich atmosphere for GJ 1132 b, placing an upper limit on the H outflow rate of $\sim 10^9$ g s^{-1} (Waalkes et al. 2019).

While cloud-free H_2-rich atmospheres are disfavored for the sample of planets studied so far, many other compositions have smaller spectral features that are still consistent with the available

data. In particular, high mean molecular weight atmospheres, made primarily of heavier molecules such as N_2, H_2O, or CO_2, have spectral features one-tenth as large as that of an H_2-dominated atmosphere. These high mean molecular weight models are well within current measurement uncertainties. In addition, small spectral features could arise from high-altitude clouds or hazes that block the transmission of stellar flux through the atmosphere and have been detected on larger gaseous planets (e.g., Kreidberg et al. 2014). Finally, a featureless spectrum is also expected if there is no atmosphere at all. Higher-precision data are needed to distinguish between these possibilities.

Some of the measured spectra show hints of H_2O features, but these features are likely due to contamination from an imhomogeneous stellar photosphere (expected for cool stars; Rackham et al. 2018). For TRAPPIST-1, the combined spectrum of planets b–g shows an inverted water absorption signature that is consistent with H_2O features in stellar faculae. The transmission spectrum of LHS 1140 b also has a marginally significant (2.65σ), noninverted water feature, but this too is consistent with expectations for stellar contamination (Edwards et al. 2021). For planets around the coolest stars, H_2O contamination from an imhomogeneous photosphere may be the norm and should be taken into account in the analysis of the spectra (Iyer & Line 2020).

Observation of the planet during secondary eclipse and other phases provides a complementary approach to transmission spectroscopy. These measurements probe the global climate and heat circulation on the planet, which can be used to estimate the surface pressure (Selsis et al. 2011, Koll et al. 2019). Thick atmospheres circulate heat more efficiently, so the higher the surface pressure is, the smaller the day–night temperature contrast will be. Thermal emission and reflection can also constrain the planet's albedo, which can reveal the presence of reflective clouds in an atmosphere and/or surface ices (e.g., Mansfield et al. 2019).

Only one planet with an M-dwarf host has been feasible for thermal emission measurements so far: LHS 3844 b, a 1.3-$R_\oplus$ planet with an 11-h orbital period. As noted in Section 5, *Spitzer* observations at 4.5 μm revealed a symmetric, large-amplitude thermal phase curve (**Figure 10**). The large day–night temperature contrast ruled out the presence of a thick (>10 bar) atmosphere on the planet (Kreidberg et al. 2019). Less massive atmospheres are expected to erode by stellar wind (see Section 2) over gigayear timescales, so the planet is most likely a bare rock with a dark, highly absorptive surface.

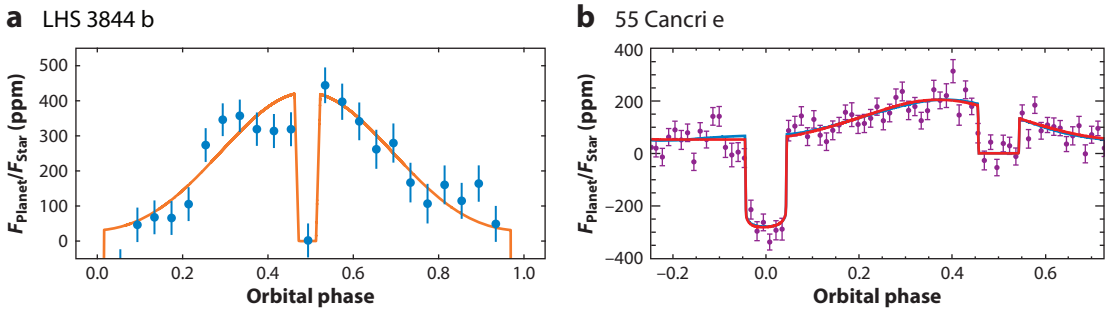

Figure 10

Thermal phase curves and best-fit models for the exoplanets (*a*) LHS 3844 b and (*b*) 55 Cancri e obtained from *Spitzer* observations. The large-amplitude, symmetric phase variation of LHS 3844 b is consistent with that expected for a bare rock. By contrast, the asymmetric phase curve of 55 Cancri e may be caused by heat circulation in an atmosphere. Figure adapted from Kreidberg et al. (2019) and Demory et al. (2016a).

6.2. Ultrashort-Period Planets with Sun-Like Host Stars

The super-Earth 55 Cancri e is a notable outlier in the population of small planets that have been studied to date. It orbits a Sun-like host star ($R_s = 0.96 R_{sun}$) every 17.7 h, resulting in a very high equilibrium temperature (around 2,000 K). The planet's bulk composition is also unusual. With a radius $R_p = 1.947 \pm 0.038\, R_\oplus$, 55 Cancri e is marginally (1.5σ) larger than predicted for a pure silicate planet with no Fe core (Crida et al. 2018), implying that it lies on the boundary between rocky and gaseous. Alternatively, it could have an interior enriched in Ca and Al, which are less dense than rock (Dorn et al. 2019). On the basis of these measurements, it is still uncertain whether the planet has a rocky surface or a thick volatile envelope.

Thanks to its high temperature and very bright host star (visible with the naked eye), 55 Cancri e is a feasible target for atmosphere characterization and has been extensively studied. The emerging consensus from transit spectroscopy measurements is that 55 Cancri e does not have a low mean molecular weight atmosphere rich in H and He. At the very high temperatures on the planet, any residual H or He in the atmosphere is expected to rapidly escape and form an extended exosphere around the planet (as observed for hot gaseous exoplanets, e.g., GJ 436 b; Ehrenreich et al. 2015). Transit observations of 55 Cancri e in Lyman α and the metastable He 1,083 nm line have yielded nondetections, placing upper limits on the H–He mass loss rates that are below those expected from low mean molecular weight compositions (Ehrenreich et al. 2012, Zhang et al. 2021). High-resolution transmission spectroscopy also places tight upper limits on C- and N-bearing molecules in an H_2-rich atmosphere (e.g., <0.001% HCN by volume; Deibert et al. 2021). One exception to these results is the low-resolution *HST*/WFC3 transmission spectrum, which hinted at an HCN feature in a low mean molecular weight atmosphere (Tsiaras et al. 2016). However, the HCN feature is marginally significant, and the retrieved abundance is inconsistent with the upper limit later obtained by Deibert et al. (2021). Overall, these results agree with theoretical predictions that an H_2-dominated atmosphere would be removed by XUV-driven loss on such a highly irradiated planet (see Section 2).

Thermal emission measurements of 55 Cancri e provide some additional insight into its atmospheric properties. One of the most intriguing observations of the planet is its thermal phase curve, measured by *Spitzer* at 4.5 μm (**Figure 10**). The phase curve shows a large day–night temperature contrast and a significantly offset hot spot ($41 \pm 12°$ east of the substellar point; Demory et al. 2016a). The maximum hemisphere-averaged temperate is $2{,}700 \pm 270$ K, and the nightside temperature is $1{,}380 \pm 400$ K. These measurements require both poor heat redistribution (to explain the large day–night contrast) and strong dayside circulation (to explain the hot spot offset). This could be due to the atmosphere having a moderate mean molecular weight (N_2 or CO) and a surface pressure of a few bars (Angelo & Hu 2017, Hammond & Pierrehumbert 2017). Low-viscosity magma flows have also been suggested as a possible explanation for the phase curve, but it is not certain that such flows could transport enough heat to fully explain the data (Demory et al. 2016a).

The IR eclipse depth of 55 Cancri e is also variable over timescales of few months, perhaps due to volcanic activity affecting the temperature structure of the upper atmosphere (Demory et al. 2016b). The nature of this variability and its origins remain poorly constrained, and additional data are needed to resolve this and other open questions surrounding the planet's atmosphere. Fortunately, 55 Cancri e is scheduled to be observed by *JWST* in its first cycle of operations, so additional constraints are forthcoming.

In addition to 55 Cancri e, there are a few other ultrashort-period rocky planets with secondary eclipse detections. These planets are below 1.6 Earth radii and thus are expected to be rocky in composition (Rogers 2015). With equilibrium temperatures above 2,000 K, their surfaces are

expected to be molten, leading to tenuous gas-melt equilibrium atmospheres (Schaefer & Fegley 2009, Miguel et al. 2011, Ito et al. 2015). One well-known example is Kepler-10b, which has a relatively large eclipse depth indicative of a high geometric albedo (0.61 ± 0.17; Batalha et al. 2011). Such a high albedo could be caused by clouds or unusually reflective lava (Rouan et al. 2011, Essack et al. 2020). By contrast, other hot rocky planets appear to have low albedo values, consistent with zero (Sheets & Deming 2017).

7. FUTURE PROSPECTS

7.1. The Next Decade of Observations

Over the next decade, many new telescopes are slated for first light, both in space and on the ground. The first is *JWST*, scheduled to launch in late 2021. With a 6.5-m-diameter mirror, *JWST* will have more than seven times the collecting area of *HST*. Its wavelength coverage also extends farther into the IR, with spectroscopic capability out to 12 μm. In addition, there are several next-generation ground-based telescopes, including the Extremely Large Telescope, the Giant Magellan Telescope, and the Thirty Meter Telescope. These have aperture sizes ranging from 24 to 39 m, offering an order-of-magnitude increase in collecting area compared with the current generation of ground-based facilities, as well as better angular resolution. These new telescopes will enable revolutionary advances in our ability to study the atmospheres of rocky worlds.

In its first year of operation, *JWST* is scheduled to observe a sample of roughly 20 rocky planets, over a range of equilibrium temperatures from 170 K (TRAPPIST-1 h) to 2,150 K (K2-141 b). These observations will provide a first glimpse of the atmospheric properties of rocky worlds in a much greater diversity of environments than we have in the Solar System. In particular, *JWST* observations of transiting planets with M-dwarf hosts will enable the first detection of several strongly absorbing molecules in the NIR, such as CO_2, H_2O, and CH_4. These molecules may be detectable with a modest number of transits or eclipses (fewer than 10) for a small sample of the most favorable planets (Barstow & Irwin 2016, Morley et al. 2017, Batalha et al. 2018, Krissansen-Totton et al. 2018, Lustig-Yaeger et al. 2019b, Wunderlich et al. 2019, Gialluca et al. 2021). H_2O and CO_2 isotopologs may also be detectable for certain atmospheric compositions (Lincowski et al. 2019). However, species with weaker or narrower absorption features, such as O_2 and O_3, will likely require dozens of transits to detect (Lustig-Yaeger et al. 2019b). Small, Earth-like concentrations of these species may be unfeasibly time intensive to detect. If clouds are present, they may truncate the amplitude of spectral features and increase the number of transits required by a factor of 10 or more (Barstow et al. 2016, Komacek et al. 2020, Suissa et al. 2020).

To circumvent the challenge of clouds, an alternative approach is emission spectroscopy. This technique probes deeper in the atmosphere thanks to the direct viewing angle (Lustig-Yaeger et al. 2019a) and is not sensitive to inhomogeneities in the stellar photosphere (Rackham et al. 2018). Thermal emission measurements have the added benefit that they are sensitive to atmospheric heat redistribution (Selsis et al. 2011, Koll & Abbot 2016, Kreidberg & Loeb 2016) or spectral features from a rocky surface, in cases where no atmosphere is present (Hu et al. 2012). This technique is most feasible for hot planets, with equilibrium temperatures above 300 K. For these planets, *JWST* could distinguish between an ~1 bar atmosphere and a bare rock in roughly 100 systems (Koll et al. 2019). For a few of the planets with the highest signal-to-noise ratio, it may also be possible to distinguish between the dominant chemical species in their atmospheres, provided that they are optically thick and not too cloudy (Morley et al. 2017).

In addition to *JWST*, there is a major push for ground-based instrumentation that can characterize rocky planet atmospheres. In the next decade, the first 30-m-class ground-based telescopes will become available. These facilities will have both higher spectral resolution and higher angular

resolution than any space-based optical/IR telescope. High-spectral-resolution studies may be capable of detecting a broad range of molecules, including species such as HDO (Mollière & Snellen 2019) or even O_2 (Snellen et al. 2013, Rodler & López-Morales 2014). While O_2 on a temperate planet is a particularly challenging case, expected to require dozens of transit observations even for the most optimistic scenarios, the observing time can be substantially decreased by combining high spectral resolution with high-contrast imaging to reduce the stellar light (Snellen et al. 2015, Lovis et al. 2017). Other molecules with a greater number of absorption lines will also be easier to detect, as will features in the atmospheres of hotter planets. High-spectral-resolution observations will thus play an important complementary role to *JWST*, particularly if the atmospheres of rocky planets are often cloudy. High-resolution observations probe the cores of absorption lines, which form higher in the atmosphere, possibly above the clouds (Gandhi et al. 2020, Hood et al. 2020). Another advantage of high-spectral-resolution data is that the planet signal is Doppler shifted relative to stellar absorption lines, which can rule out stellar contamination that can affect low-resolution observations (Rackham et al. 2018). Finally, if the signal-to-noise ratio is high enough, it may even be possible to estimate wind speeds from the Doppler shift of the lines, as has been done for hot Jupiters (Snellen et al. 2010).

7.2. Testing Regime Diagrams of Rocky Planet Atmospheres

The coming wave of new observations will soon make it possible to test regime diagrams of rocky exoplanet atmospheres. **Figure 11** depicts one such diagram, building on previous research by Forget & Leconte (2014) and Zahnle & Catling (2017). The diagram axes are equilibrium temperature and planetary radius, because these two parameters are particularly critical to evolution (although clearly many other parameters are also important). A horizontal line on the plot at $R = 1.6\ R_\oplus$ divides sub-Neptunes from rocky planets on the basis of the empirical evidence discussed in Section 1 (Weiss & Marcy 2014, Rogers 2015, Wolfgang & Lopez 2015). The vertical lines indicate condensation temperatures of key species,[3] which strongly influence bulk atmospheric composition (see Section 1.3).

Broadly speaking, planets and satellites shown at the bottom right of **Figure 11** are expected to be airless. The sloped lines indicate two possible boundaries for this transition. The dashed line is based on the empirical "cosmic shoreline" of Zahnle & Catling (2017), for which the stellar flux–escape velocity scaling is given by $F \propto v_{esc}^4$ (Section 2.3). Given $F \propto T_{eq}^4$, this implies $v_{esc} \propto T_{eq}$. The dotted line follows $v_{esc}^2 \propto T_{eq}$, which would apply for hydrodynamic escape given linear proportionality between T_{eq} and the upper atmosphere temperature, and a transition to rapid escape at some critical λ value.[4] Both lines assume Earth-like rocky composition to obtain v_{esc} as a function of radius (Zeng et al. 2019) and are normalized to Mars, a planet that has almost but not quite lost its entire atmosphere.

Perhaps the most striking aspect of **Figure 11** is that all the rocky exoplanets shown are in a distinct region of parameter space compared with both Solar System bodies and larger exoplanets.

[3] Condensation temperature is calculated at 300 Pa for N_2, CO_2, and H_2O. This choice is somewhat arbitrary, but it ensures that the H_2O condensation temperature (266 K) is close to the runaway greenhouse equilibrium temperature limit (Goldblatt et al. 2013). Above the condensation temperature of a given species, atmospheric abundance increases rapidly until the surface reservoir is exhausted. The condensation line for H_2SO_4 is included because of its importance to atmospheric aerosols, with a value of 400 K (following Lincowski et al. 2018).

[4] This relationship can be seen by combining the definitions of λ (Equation 1) and escape velocity, $v_{esc} \equiv \sqrt{2GM/R}$.

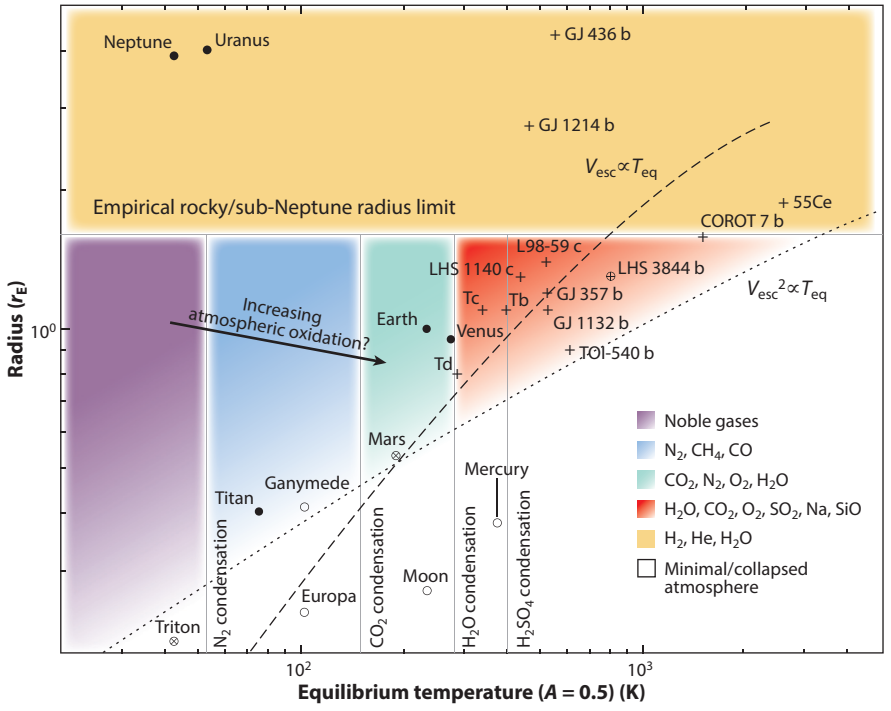

Figure 11

Regime diagram of plausible rocky planet atmospheric compositions as a function of equilibrium temperature (assuming an albedo of 0.5) and radius. Filled circles represent Solar System planets and moons with stable atmospheres, crossed circles represent those with collapsed atmospheres, and open circles represent those without atmospheres. Plus signs represent selected exoplanets from **Table 1**, and an open circle representing LHS 3844 b indicates its low inferred atmospheric pressure. The legend indicates plausible dominant atmospheric constituents for each region of the diagram. The dashed and dotted lines indicate theoretical curves for total atmospheric loss. The horizontal line at $R = 1.6\ R_\oplus$ divides sub-Neptunes from rocky planets. The vertical lines indicate condensation temperatures of key species. The rocky exoplanets amenable to near-future characterization occupy a region of parameter space that is not observed in the Solar System. Abbreviations: Tb, Tc, and Td, TRAPPIST-1 b, c, and d, respectively; 55Ce, 55 Cancri e.

Characterizing the atmospheres of these planets will allow us to tackle vital new questions in rocky exoplanet evolution:

1. What is the dependence of the $1.6\ R_\oplus$ sub-Neptune/rocky boundary on equilibrium temperature? Both exoplanet mass–radius statistics (Fulton & Petigura 2018) and the nondetection of an H_2–He atmosphere on 55 Cancri e suggest that highly irradiated planets lose more H than less irradiated ones, but more data are needed.
2. Where does the airless boundary for rocky planets occur, and how much scatter in this boundary is driven by other factors such as star type? Existing observations of LHS 3844 b (Kreidberg et al. 2019) have already provided clues, but many more data are needed to characterize this transition comprehensively.
3. What are the key transitions in atmospheric composition above $T_{eq} = 300$ K? Rocky planets with atmospheres in this regime have no direct analog in the Solar System, so for the moment we have only theory to guide us.

4. Is there an observable trend toward more oxidizing atmospheres at higher T_{eq} and lower radius due to H loss, as expected from theory?

All of these questions provide strong motivation for future observational campaigns.

7.3. Habitability and Biosignatures

Searching for life on exoplanets is the most exciting future goal of all. The philosophical significance of the discovery of life on another world defies superlatives: It would be the most important breakthrough since the Copernican revolution at least. The challenges to be surmounted remain considerable. Nonetheless, the prospect of characterizing the habitability and potential biospheres of nearby rocky exoplanets is getting ever closer, and enormous strides forward are expected in the coming years.

In the Solar System, we have only a single known example of an inhabited planet, so any attempt to predict habitability for exoplanets is by necessity an extrapolation. While the debate about how to define life is ongoing, most studies of exoplanet habitability use the universal dependence of known life on liquid water and organic carbon chemistry as a starting point. Extensive research has been performed to define the habitable zone, or the range of distances from a host star over which a planet may support surface liquid water (e.g., Kasting et al. 1993, Selsis et al. 2007, Abe et al. 2011, Pierrehumbert & Gaidos 2011, Kopparapu et al. 2013, Seager 2013, Shields et al. 2016, Ramirez 2018). The now-canonical definition of the habitable zone, which was proposed by Kasting et al. (1993), is the range of distances over which an Earth-like planet can sustain surface liquid water while CO_2 is a noncondensing atmospheric constituent. It therefore corresponds roughly to the region between the CO_2 and H_2O condensation lines in **Figure 11**. The motivation for this definition is the carbonate–silicate cycle, which is believed to have regulated Earth's surface temperature via CO_2 changes on geologic timescales (Walker et al. 1981). This definition may require a planet to possess Earth-like plate tectonics (Seager 2013, Kasting et al. 2014), and CO_2 warming alone cannot explain the evidence for surface liquid water on Mars three to four billion years ago (Wordsworth 2016b). As a result, many other habitable zone definitions have been proposed using various alternative assumptions (see the references cited above for details).

Although the validity of the habitable zone concept is still debated (e.g., Moore et al. 2017), it has proved popular in the exoplanet community, and investigations of exoplanet habitability under different scenarios have indirectly helped to improve our understanding of planetary evolution in the Solar System. Some recent studies have considered how the habitable zone could be tested observationally. Bean et al. (2017) proposed a statistical approach via low-resolution observations of CO_2 abundances on a large number of rocky exoplanets. However, other authors have suggested the observational challenges will be severe, even for next-generation telescopes (Lehmer et al. 2020).

An alternative test of rocky exoplanet habitability that avoids a priori assumptions about CO_2 regulation is to look for surface liquid water directly. One possibility is to look for signs of ocean glint using a high-contrast direct-imaging telescope (Robinson et al. 2010, Lustig-Yaeger et al. 2018). Aqueous chemistry may also be used to constrain surface liquid water abundances indirectly, for example, via a planet's sulfur cycle (Loftus et al. 2019) or possibly its ammonia inventory (Hu et al. 2021). While liquid water is essential for Earth-like life, too much water may be detrimental to habitability because of how it affects volatile sequestration (Kitzmann et al. 2015, Marounina & Rogers 2020), outgassing (Krissansen-Totton et al. 2021b), and near-surface nutrient availability (Wordsworth & Pierrehumbert 2013b, Glaser et al. 2020). Techniques to determine surface pressure and temperature, and ultimately to detect surface land masses directly, will therefore be important as well (Cowan et al. 2009, Benneke & Seager 2012).

While liquid water is fundamental to habitability, the redox chemistry of a rocky planet is critical to its chances of developing life in the first place. As they lose H_2 to space, many rocky planets may pass through a stage where both liquid water and reducing chemistry allowing formation of prebiotic compounds are present (Wordsworth 2012, Luger et al. 2015). However, on planets where H_2O photolysis and H loss continue once all H_2 is lost, the resulting hyperoxidation of the atmosphere and surface will cause organic compounds to be rapidly destroyed by oxidants, likely preventing the emergence and survival of Earth-like life. The best targets for life searches may therefore be those planets that have undergone just enough H escape to remove their primordial H_2 envelopes, but not enough to hyperoxidize their surfaces.

Redox is also critical to the topic of biosignatures (Seager et al. 2012). Biosignature definition is an important topic that has been covered in detail in several comprehensive recent reviews (e.g., Kaltenegger 2017, Meadows et al. 2018, Schwieterman et al. 2018). In brief, the classic approach to biosignature definition relies on the idea that life pushes planetary atmospheres toward increasing chemical disequilibrium (Lovelock 1965), leading to the simultaneous presence of oxidizing and reducing atmospheric species (e.g., O_2 and CH_4 on Earth). However, the last few years of research have made it clear that many such gases, particularly O_2, can also be produced by abiotic processes. Biosignature definition has therefore moved from a focus on close Earth analogs to a broader view that encompasses the possibility of a wide variety of atmospheric redox states, metabolisms, and signature gases (e.g., Catling et al. 2018, Olson et al. 2018, Sousa-Silva et al. 2020).

Research in this area is ongoing, but two main themes are now clear. First, while detection of a single molecule is unlikely to constitute a "smoking gun" biosignature alone, observations of multiple species in the atmosphere of a single target can be used to build an increasingly convincing case that a biosphere is present, particularly when additional context is provided. Second, the more we understand how rocky exoplanet atmospheres evolve in the absence of a biosphere, the stronger the case for life will be when biosignatures are detected. The next decade of atmospheric characterization will therefore be a critical phase on the road to detecting life outside our Solar System.

7.4. Observing Biosignatures with a Next-Generation Telescope

There is broad consensus in the exoplanet community that a next-generation direct imaging mission is needed to detect biosignatures in the atmospheres of Earth-mass planets orbiting Sun-like stars (Dalcanton et al. 2015, Natl. Acad. Sci. Med. 2018). While the next decade will see major steps forward in identifying the basic atmospheric chemistry and climate of rocky exoplanets, almost all of these planets have M-dwarf host stars (**Table 1**). Even for these systems, *JWST* and the extremely large telescopes will be hard pressed to identify biosignatures. For example, O_2 may be detectable on a handful of the most accessible planets with intensive observing campaigns (TRAPPIST-1 e or Proxima b); however, the simulated detections rely on optimistic assumptions about the O_2 concentration and presence of clouds in the atmosphere. Even if O_2 were detected, it is not a biosignature on its own. To robustly detect biospheres, a more complete chemical inventory is therefore needed, for a larger sample of planets with a broader range of host star types.

To bridge this gap, several ambitious, next-generation space missions have recently been proposed with the goal of searching for biosignatures on a large sample (approximately dozens) of temperate rocky planets. These include *HABEx* (*Habitable Exoplanet Observatory*), *LUVOIR* (*Large UV/Optical/IR Surveyor*), and *LIFE* (*Large Interferometer for Exoplanets*) (LUVOIR Team 2019, Gaudi et al. 2020, Quanz et al. 2021). The proposed facilities would use a variety of technologies to achieve the high contrast and high angular resolution required for direct imaging of other Earths: starlight suppression with a coronograph or a starshade, or interferometry. These projects

build on the heritage of many previously studied missions, notably the *Terrestrial Planet Finder* and *Darwin* concepts (Defrère et al. 2018).

Now that the occurrence rate of temperate rocky planets is known (Dressing & Charbonneau 2015, Bryson et al. 2021), the time is ripe to pursue a flagship mission to characterize them in more detail. A space-based exoplanet imaging mission was recommended as the top scientific priority by both the US-based 2020 decadal survey on astronomy and astrophysics (Natl. Acad. Sci. Med. 2021) and the European Space Agency's Voyage 2050 report. Specifically, the 2020 decadal survey recommended a large (~6-m-aperture) IR/optical/UV space telescope to launch in the mid-2040s; such a mission could obtain spectra of 25 potentially habitable exoplanets. Similarly, the Voyage 2050 report recommended an exoplanet interferometry mission, if it proves to be financially feasible. The 2020 decadal survey also recognized the technical challenge and potential high cost of the proposed imaging missions and laid out a multidecade path that begins with an aggressive program of technology maturation for the 2020s.

With these recommendations, we are poised to finally address an age-old question: Is there alien life around other stars? Exoplanet science has witnessed enormous progress in the three short decades of its existence, and with an ambitious strategy, hard work from a growing community, and international collaboration, the next 30 years will be even more exciting. We have already learned that exoplanets are more diverse and varied in their properties than we had ever imagined from the small sample in the Solar System. In this review we have presented a snapshot of the current view of rocky exoplanet atmospheres, but if history is any guide, we can expect that this article will quickly go out of date as we continue on the path to characterizing Earth-like worlds.

DISCLOSURE STATEMENT

The authors are not aware of any affiliations, memberships, funding, or financial holdings that might be perceived as affecting the objectivity of this review.

ACKNOWLEDGMENTS

Comprehensively covering such an exciting and fast-moving new field in a single review is a great challenge, and we apologize to any colleagues whose work we inadvertently omitted. We thank Collin Cherubim, Jess Cmiel, Hannah Diamond-Lowe, Feng Ding, Kait Loftus, Laura Schaefer, Jake Lustig-Yaeger, Kevin Zahnle, and an anonymous reviewer for discussion and comments that greatly improved the manuscript. This research has made extensive use of NASA's Astrophysics Data System and the NASA Exoplanet Archive. R.W. acknowledges funding from a National Science Foundation CAREER award (AST-1847120) and Virtual Planetary Laboratory award UWSC10439. L.K. acknowledges generous support from the Max Planck Society.

LITERATURE CITED

Abbot DS, Cowan NB, Ciesla FJ. 2012. *Astrophys. J.* 756(2):178–90
Abe Y, Abe-Ouchi A, Sleep NH, Zahnle KJ. 2011. *Astrobiology* 11(5):443–60
Airapetian VS, Glocer A, Gronoff G, Hebrard E, Danchi W. 2016. *Nat. Geosci.* 9(6):452–55
Angelo I, Hu R. 2017. *Astron. J.* 154(6):232
Anglada-Escudé G, Amado PJ, Barnes J, et al. 2016. *Nature* 536(7617):437–40
Ardaseva A, Rimmer PB, Waldmann I, et al. 2017. *MNRAS* 470(1):187–96
Armstrong K, Frost DJ, McCammon CA, Rubie DC, Ballaran TB. 2019. *Science* 365(6456):903–6
Arney GN, Meadows VS, Domagal-Goldman SD, et al. 2017. *Astrophys. J.* 836(1):49
Arnscheidt CW, Wordsworth RD, Ding F. 2019. *Astrophys. J.* 881(1):60
Auclair-Desrotour P, Heng K. 2020. *Astron. Astrophys.* 638:A77

Baraffe I, Homeier D, Allard F, Chabrier G. 2015. *Astron. Astrophys.* 577:A42
Barstow JK, Aigrain S, Irwin PGJ, Kendrew S, Fletcher LN. 2016. *MNRAS* 458(3):2657–66
Barstow JK, Irwin PGJ. 2016. *MNRAS* 461(1):L92–96
Batalha NE, Lewis NK, Line MR, Valenti J, Stevenson K. 2018. *Astrophys. J. Lett.* 856(2):L34
Batalha NM, Borucki WJ, Bryson ST, et al. 2011. *Astrophys. J.* 729(1):27
Batalha NM, Rowe JF, Bryson ST, et al. 2013. *Astrophys. J. Suppl. Ser.* 204(2):24
Bean JL, Abbot DS, Kempton EMR. 2017. *Astrophys. J. Lett.* 841(2):L24
Bean JL, Raymond SN, Owen JE. 2021. *J. Geophys. Res. Planets* 126:e06639
Bedell M, Bean JL, Meléndez J, et al. 2018. *Astrophys. J.* 865(1):68
Benneke B, Seager S. 2012. *Astrophys. J.* 753(2):100
Berger TA, Huber D, Gaidos E, van Saders JL, Weiss LM. 2020. *Astron. J.* 160(3):108
Berner RA. 2004. *The Phanerozoic Carbon Cycle: CO_2 and O_2*. Oxford, UK: Oxford Univ. Press
Bolmont E, Selsis F, Owen JE, et al. 2017. *MNRAS* 464(3):3728–41
Brain DA, Jakosky BM. 1998. *J. Geophys. Res. Planets* 103(10):E22689–94
Bryson S, Kunimoto M, Kopparapu RK, et al. 2021. *Astron. J.* 161(1):36
Buchhave LA, Latham DW. 2015. *Astrophys. J.* 808(2):187
Carone L, Baeyens R, Mollière P, et al. 2020. *MNRAS* 496(3):3582–614
Carone L, Keppens R, Decin L. 2014. *MNRAS* 445(1):930–45
Carone L, Keppens R, Decin L. 2015. *MNRAS* 453(3):2412–37
Carone L, Keppens R, Decin L. 2016. *MNRAS* 461(2):1981–2002
Carroll JJ, Slupsky JD, Mather AE. 1991. *J. Phys. Chem. Ref. Data* 20(6):1201–9
Castan T, Menou K. 2011. *Astrophys. J. Lett.* 743(2):L36
Catling DC, Krissansen-Totton J, Kiang NY, et al. 2018. *Astrobiology* 18(6):709–38
Catling DC, Zahnle KJ, McKay CP. 2001. *Science* 293(5531):839–43
Chachan Y, Stevenson DJ. 2018. *Astrophys. J.* 854(1):21
Chapman S, Cowling TG. 1970. *The Mathematical Theory of Non-Uniform Gases: An Account of the Kinetic Theory of Viscosity, Thermal Conduction and Diffusion in Gases*. Cambridge, UK: Cambridge Univ. Press
Checlair JH, Menou K, Abbot DS. 2017. *Astrophys. J.* 845(2):132
Checlair JH, Olson SL, Jansen MF, Abbot DS. 2019. *Astrophys. J. Lett.* 884(2):L46
Chen H, Wolf ET, Zhan Z, Horton DE. 2019. *Astrophys. J.* 886(1):16
Coltice N, Schmalzl J. 2006. *Geophys. Res. Lett.* 33(23). **https://doi.org/10.1029/2006GL027707**
Cowan NB, Agol E, Meadows VS, et al. 2009. *Astrophys. J.* 700(2):915
Crida A, Ligi R, Dorn C, Borsa F, Lebreton Y. 2018. *Res. Notes Am. Astron. Soc.* 2(3):172
Crosley MK, Osten RA. 2018. *Astrophys. J.* 856(1):39
Dalcanton J, Seager S, Aigrain S, et al. 2015. arXiv:1507.04779 [astro-ph]
de Wit J, Wakeford HR, Gillon M, et al. 2016. *Nature* 537(7618):69–72
de Wit J, Wakeford HR, Lewis NK, et al. 2018. *Nat. Astron.* 2:214–19
Defrère D, Absil O, Beichman CA. 2018. In *Handbook of Exoplanets*, ed. HJ Deeg, JA Belmonte, pp. 1229–55. Cham, Switz.: Springer
Deibert EK, de Mooij EJW, Jayawardhana R, et al. 2021. *Astrophys. J.* 161(5):209
Demory BO, Gillon M, de Wit J, et al. 2016a. *Nature* 532(7598):207–9
Demory BO, Gillon M, Madhusudhan N, Queloz D. 2016b. *MNRAS* 455(2):2018–27
Deng J, Du Z, Karki BB, Ghosh DB, Lee KKM. 2020. *Nat. Commun.* 11:2007
Desch SJ, Abbot D, Krijt S, et al. 2020. In *Planetary Diversity*, ed. EJ Tasker, C Unterborn, M Laneuville, et al., pp. 6-1–6-40. Bristol, UK: IOP Sci.
DeWitt HL, Hasenkopf CA, Trainer MG, et al. 2010. *Astrobiology* 10(8):773–81
Diamond-Lowe H, Berta-Thompson Z, Charbonneau D, Dittmann J, Kempton EMR. 2020a. *Astrophys. J.* 160(1):27
Diamond-Lowe H, Berta-Thompson Z, Charbonneau D, Kempton EMR. 2018. *Astrophys. J.* 156(2):42
Diamond-Lowe H, Charbonneau D, Malik M, Kempton EMR, Beletsky Y. 2020b. *Astrophys. J.* 160(4):188
Ding F, Pierrehumbert RT. 2016. *Astrophys. J.* 822(1):24
Ding F, Pierrehumbert RT. 2018. *Astrophys. J.* 867(1):54

Ding F, Wordsworth RD. 2020. *Astrophys. J. Lett.* 891(1):L18
Domagal-Goldman SD, Kasting JF, Johnston DT, Farquhar J. 2008. *Earth Planet. Sci. Lett.* 269(1/2):29–40
Dong C, Jin M, Lingam M, et al. 2018. *PNAS* 115(2):260–65
Dorn C, Harrison JHD, Bonsor A, Hands TO. 2019. *MNRAS* 484(1):712–27
Dressing CD, Charbonneau D. 2015. *Astrophys. J.* 807(1):45
Edwards B, Changeat Q, Mori M, et al. 2021. *Astrophys. J.* 161(1):44
Ehrenreich D, Bourrier V, Bonfils X, et al. 2012. *Astron. Astrophys.* 547:A18
Ehrenreich D, Bourrier V, Wheatley PJ, et al. 2015. *Nature* 522(7557):459–61
Elkins-Tanton LT. 2012. *Annu. Rev. Earth Planet. Sci.* 40:113–39
Essack Z, Seager S, Pajusalu M. 2020. *Astrophys. J.* 898(2):160
Etiope G, Ehlmann BL, Schoell M. 2013. *Icarus* 224(2):276–85
Fazio GG, Hora JL, Allen LE, et al. 2004. *Astrophys. J. Suppl. Ser.* 154(1):10–17
Fegley B, Zolotov MY, Lodders K. 1997. *Icarus* 125(2):416–39
Feng YK, Robinson TD, Fortney JJ, et al. 2018. *Astron. J.* 155(5):200
Ferris JP, Joshi PC, Edelson EH, Lawless JG. 1978. *J. Mol. Evol.* 11(4):293–311
Fischer RA, Campbell AJ, Shofner GA, et al. 2011. *Earth Planet. Sci. Lett.* 304(3/4):496–502
Fischer RA, Cottrell E, Hauri E, Lee KKM, Le Voyer M. 2020. *PNAS* 117(16):8743–49
Forget F, Leconte J. 2014. *Philos. Trans. R. Soc. A* 372(2014):20130084
Forget F, Pierrehumbert RT. 1997. *Science* 278(5341):1273–76
France K, Loyd ROP, Youngblood A, et al. 2016. *Astrophys. J.* 820(2):89
Fulton BJ, Petigura EA. 2018. *Astron. J.* 156(6):264
Fulton BJ, Petigura EA, Howard AW, et al. 2017. *Astron. J.* 154(3):109
Gaillard F, Bernadou F, Roskosz M, et al. 2022. *Earth Planet. Sci. Lett.* 577:117255
Gandhi S, Brogi M, Webb RK. 2020. *MNRAS* 498(1):194–204
Gao P, Benneke B. 2018. *Astrophys. J.* 863(2):165
Gao P, Hu R, Robinson TD, Li C, Yung YL. 2015. *Astrophys. J.* 806(2):249
García Muñoz A, Fossati L, Youngblood A, et al. 2021. *Astrophys. J. Lett.* 907(2):L36
Garcia-Sage K, Glocer A, Drake JJ, Gronoff G, Cohen O. 2017. *Astrophys. J. Lett.* 844(1):L13
Gaudi BS, Seager S, Mennesson B, et al. 2020. arXiv:2001.06683 [astro-ph]
Gialluca MT, Robinson TD, Rugheimer S, Wunderlich F. 2021. *Publ. Astron. Soc. Pac.* 133:054401
Gillon M, Triaud AHMJ, Demory BO, et al. 2017. *Nature* 542(7642):456–60
Ginzburg S, Schlichting HE, Sari R. 2018. *MNRAS* 476(1):759–65
Glaser DM, Hartnett HE, Desch SJ, et al. 2020. *Astrophys. J.* 893(2):163
Goldblatt C, Claire MW, Lenton TM, et al. 2009. *Nat. Geosci.* 2(12):891–96
Goldblatt C, Robinson TD, Zahnle KJ, Crisp D. 2013. *Nat. Geosci.* 6(8):661–67
Gómez-Leal I, Kaltenegger L, Lucarini V, Lunkeit F. 2019. *Icarus* 321:608–18
Greaves JS, Richards A, Bains W, et al. 2021. *Nat. Astron.* 5(7):655–64
Grewal DS, Dasgupta R, Farnell A. 2020. *Geochim. Cosmochim. Acta* 280:281–301
Gunell H, Maggiolo R, Nilsson H, et al. 2018. *Astron. Astrophys.* 614:L3
Gupta A, Schlichting HE. 2019. *MNRAS* 487(1):24–33
Hakim K, Van den Berg A, Vazan A, et al. 2019. *Astron. Astrophys.* 630:A152
Hamano K, Abe Y, Genda H. 2013. *Nature* 497(7451):607–10
Hammond M, Pierrehumbert RT. 2017. *Astrophys. J.* 849(2):152
Haqq-Misra J, Kopparapu RK, Batalha NE, Harman CE, Kasting JF. 2016. *Astrophys. J.* 827(2):120
Hawkesworth CJ, Brown M. 2018. *Philos. Trans. R. Soc. A* 376(2132):20180228
Hayashi C, Nakazawa K, Mizuno H. 1979. *Earth Planet. Sci. Lett.* 43(1):22–28
He C, Hörst SM, Lewis NK, et al. 2020. *Nat. Astron.* 4(10):986–93
Hébrard E, Bénilan Y, Raulin F. 2005. *Adv. Space Res.* 36(2):268–73
Heller R, Leconte J, Barnes R. 2011. *Astron. Astrophys.* 528:A27
Hirschmann MM. 2000. *Geochem. Geophys. Geosyst.* 1(10). **https://doi.org/10.1029/2000GC000070**
Hoffman PF, Kaufman AJ, Halverson GP, Schrag DP. 1998. *Science* 281(5381):1342–46
Höning D, Tosi N, Spohn T. 2019. *Astron. Astrophys.* 627:A48

Hood CE, Fortney JJ, Line MR, et al. 2020. *Astron. J.* 160(5):198
Hörst SM, He C, Lewis NK, et al. 2018. *Nat. Astron.* 2(4):303–6
Howard AW, Marcy GW, Bryson ST, et al. 2012. *Astrophys. J. Suppl. Ser.* 201(2):15
Hu R, Damiano M, Scheucher M, et al. 2021. *Astrophys. J. Lett.* 921(1):18
Hu R, Ehlmann BL, Seager S. 2012. *Astrophys. J.* 752(1):7
Hu R, Seager S. 2014. *Astrophys. J.* 784(1):63
Hu R, Seager S, Bains W. 2013. *Astrophys. J.* 769(1):6
Hunten DM, Pepin RO, Walker JC. 1987. *Icarus* 69(3):532–49
Hurowitz JA, Fischer WW, Tosca NJ, Milliken RE. 2010. *Nat. Geosci.* 3(5):323–26
Ikoma M, Hori Y. 2012. *Astrophys. J.* 753(1):66
Ingalls JG, Krick JE, Carey SJ, et al. 2016. *Astrophys. J.* 152(2):44
Ingersoll AP. 1969. *J. Atmos. Sci.* 26(6):1191–98
Ito Y, Ikoma M, Kawahara H, et al. 2015. *Astrophys. J.* 801(2):144
Iyer AR, Line MR. 2020. *Astrophys. J.* 889(2):78
Javoy M. 1999. *C. R. Acad. Sci.* 329(8):537–55
Joshi MM. 2003. *Astrobiology* 3(2):415–27
Joshi MM, Haberle RM. 2012. *Astrobiology* 12(1):3–8
Joshi MM, Haberle RM, Reynolds RT. 1997. *Icarus* 129(2):450–65
Kaltenegger L. 2017. *Annu. Rev. Astron. Astrophys.* 55:433–85
Kaltenegger L, Sasselov D. 2009. *Astrophys. J.* 708(2):1162
Kane SR, Arney G, Crisp D, et al. 2019. *J. Geophys. Res. Planets* 124(8):2015–28
Kang W, Ding F, Wordsworth R, Seager S. 2021. *Astrophys. J.* 906(2):67
Kang W, Wordsworth R. 2019. *Astrophys. J. Lett.* 885(1):L18
Kaspi Y, Showman AP. 2015. *Astrophys. J.* 804(1):60
Kasting JF, Brown LL. 1998. In *The Molecular Origins of Life: Assembling the Pieces of the Puzzle*, ed. A Brack, pp. 35–56. New York: Cambridge Univ. Press
Kasting JF, Kopparapu R, Ramirez RM, Harman CE. 2014. *PNAS* 111(35):12641–46
Kasting JF, Liu SC, Donahue TM. 1979. *J. Geophys. Res. Oceans* 84(6):C3097–107
Kasting JF, Whitmire DP, Reynolds RT. 1993. *Icarus* 101(1):108–28
Katyal N, Ortenzi G, Grenfell JL, et al. 2020. *Astron. Astrophys.* 643:A81
Kempton EMR, Bean JL, Louie DR, et al. 2018. *Publ. Astron. Soc. Pac.* 130(993):114401
Khurana KK, Jia X, Kivelson MG, et al. 2011. *Science* 332(6034):1186–89
Kimble RA, MacKenty JW, O'Connell RW, Townsend JA. 2008. *Proc. SPIE* 7010:70101E
Kislyakova KG, Holmström M, Odert P, et al. 2019. *Astron. Astrophys.* 623:A131
Kite ES, Fegley B Jr., Schaefer L, Gaidos E. 2016. *Astrophys. J.* 828(2):80
Kite ES, Ford EB. 2018. *Astrophys. J.* 864(1):75
Kitzmann D, Alibert Y, Godolt M, et al. 2015. *MNRAS* 452(4):3752–58
Klein C. 2005. *Am. Mineral.* 90(10):1473–99
Knutson HA, Benneke B, Deming D, Homeier D. 2014. *Nature* 505(7481):66–68
Koll DDB, Abbot DS. 2016. *Astrophys. J.* 825(2):99
Koll DDB, Malik M, Mansfield M, et al. 2019. *Astrophys. J.* 886(2):140
Komacek TD, Fauchez TJ, Wolf ET, Abbot DS. 2020. *Astrophys. J. Lett.* 888(2):L20
Komacek TD, Jansen MF, Wolf ET, Abbot DS. 2019. *Astrophys. J.* 883(1):46
Kopparapu R, Wolf ET, Haqq-Misra J, et al. 2016. *Astrophys. J.* 819(1):84
Kopparapu RK, Ramirez R, Kasting JF, et al. 2013. *Astrophys. J.* 765(2):131
Korenaga J. 2010. *Astrophys. J. Lett.* 725(1):L43
Kreidberg L, Bean JL, Désert JM, et al. 2014. *Nature* 505(7481):69–72
Kreidberg L, Koll D, Morley C, et al. 2019. *Nature* 573(7772):87–90
Kreidberg L, Loeb A. 2016. *Astrophys. J. Lett.* 832(1):L12
Krissansen-Totton J, Fortney JJ, Nimmo F, Wogan N. 2021a. *AGU Adv.* 2(2):e2020AV000294
Krissansen-Totton J, Galloway ML, Wogan N, Dhaliwal JK, Fortney JJ. 2021b. *Astrophys. J.* 913(2):107
Krissansen-Totton J, Garland R, Irwin P, Catling DC. 2018. *Astron. J.* 156(3):114

Lammer H, Kasting JF, Chassefière E, et al. 2008. *Space Sci. Rev.* 139(1–4):399–436
Lammer H, Scherf M, Kurokawa H, et al. 2020. *Space Sci. Rev.* 216(4):74
Lebrun T, Massol H, Chassefière E, et al. 2013. *J. Geophys. Res. Planets* 118(6):1155–76
Leconte J, Forget F, Charnay B, et al. 2013. *Astron. Astrophys.* 554:A69
Leconte J, Wu H, Menou K, Murray N. 2015. *Science* 347(6222):632–35
Lee EJ, Chiang E. 2015. *Astrophys. J.* 811(1):41
Lefèvre M, Turbet M, Pierrehumbert R. 2021. *Astrophys. J.* 913(2):101
Lehmer OR, Catling DC, Krissansen-Totton J. 2020. *Nat. Commun.* 11:6153
Lenardic A, Crowley JW. 2012. *Astrophys. J.* 755(2):132
Levi A, Sasselov D, Podolak M. 2017. *Astrophys. J.* 838(1):24
Libby-Roberts JE, Berta-Thompson ZK, Diamond-Lowe H, et al. 2021. arXiv:2105.10487 [astro-ph]
Libourel G, Marty B, Humbert F. 2003. *Geochim. Cosmochim. Acta* 67(21):4123–35
Lichtenberg T, Bower DJ, Hammond M, et al. 2021. *J. Geophys. Res. Planets* 126:e2020JE006711
Lichtenberg T, Golabek GJ, Burn R, et al. 2019. *Nat. Astron.* 3(4):307–13
Lichtenegger HIM, Lammer H, Grießmeier JM, et al. 2010. *Icarus* 210(1):1–7
Lincowski AP, Lustig-Yaeger J, Meadows VS. 2019. *Astron. J.* 158(1):26
Lincowski AP, Meadows VS, Crisp D, et al. 2018. *Astrophys. J.* 867(1):76
Lodders K. 2003. *Astrophys. J.* 591(2):1220
Loftus K, Wordsworth RD. 2021. *J. Geophys. Res. Planets* 126:e2020JE006653
Loftus K, Wordsworth RD, Morley CV. 2019. *Astrophys. J.* 887(2):231
Lopez ED, Fortney JJ. 2013. *Astrophys. J.* 776(1):2
Lopez ED, Fortney JJ. 2014. *Astrophys. J.* 792(1):1
Lopez-Puertas M, Taylor FW. 2001. *Non-LTE Radiative Transfer in the Atmosphere*, Vol. 3. Singapore: World Sci.
Lovelock JE. 1965. *Nature* 207(997):568–70
Lovis C, Snellen I, Mouillet D, et al. 2017. *Astron. Astrophys.* 599:A16
Luger R, Barnes R. 2015. *Astrobiology* 15(2):119–43
Luger R, Barnes R, Lopez E, et al. 2015. *Astrobiology* 15(1):57–88
Luger R, Lustig-Yaeger J, Fleming DP, et al. 2017. *Astrophys. J.* 837(1):63
Lupu RE, Zahnle K, Marley MS, et al. 2014. *Astrophys. J.* 784(1):27
Lustig-Yaeger J, Meadows VS, Lincowski AP. 2019a. *Astrophys. J. Lett.* 887(1):L11
Lustig-Yaeger J, Meadows VS, Lincowski AP. 2019b. *Astron. J.* 158(1):27
Lustig-Yaeger J, Meadows VS, Mendoza GT, et al. 2018. *Astron. J.* 156(6):301
LUVOIR Team. 2019. arXiv:1912.06219 [astro-ph.IM]
Malsky I, Rogers LA. 2020. *Astrophys. J.* 896(1):48
Mansfield M, Kite ES, Hu R, et al. 2019. *Astrophys. J.* 886(2):141
Marounina N, Rogers LA. 2020. *Astrophys. J.* 890(2):107
Mayor M, Queloz D. 1995. *Nature* 378(6555):355–59
Mbarek R, Kempton EMR. 2016. *Astrophys. J.* 827(2):121
McDonald GD, Kreidberg L, Lopez E. 2019. *Astrophys. J.* 876(1):22
McKay CP, Pollack JB, Courtin R. 1991. *Science* 253(5024):1118–21
Meadows VS, Reinhard CT, Arney GN, et al. 2018. *Astrobiology* 18(6):630–62
Melosh HJ, Vickery AM. 1989. *Nature* 338(6215):487–89
Merlis TM, Schneider T. 2010. *J. Adv. Model. Earth Syst.* 2(4). **https://doi.org/10.3894/JAMES.2010.2.13**
Miguel Y, Kaltenegger L, Fegley B, Schaefer L. 2011. *Astrophys. J. Lett.* 742(2):L19
Mitri G, Showman AP, Lunine JI, Lorenz RD. 2007. *Icarus* 186(2):385–94
Mollière P, Snellen IAG. 2019. *Astron. Astrophys.* 622:A139
Moore WB, Lenardic A, Jellinek A, et al. 2017. *Nat. Astron.* 1(2):43
Morbidelli A, Lunine JI, O'Brien DP, Raymond SN, Walsh KJ. 2012. *Annu. Rev. Earth Planet. Sci.* 40:251–75
Morley CV, Kreidberg L, Rustamkulov Z, Robinson T, Fortney JJ. 2017. *Astrophys. J.* 850(2):121
Mugnai LV, Modirrousta-Galian D, Edwards B, et al. 2021. *Astrophys. J.* 161(6):284
Murray-Clay RA, Chiang EI, Murray N. 2009. *Astrophys. J.* 693(1):23

Natl. Acad. Sci. Med. 2018. *Exoplanet Science Strategy*. Washington, DC: Natl. Acad. Press
Natl. Acad. Sci. Med. 2021. *Pathways to Discovery in Astronomy and Astrophysics for the 2020s*. Washington, DC: Natl. Acad. Press
Neumann GA, Cavanaugh JF, Sun X, et al. 2013. *Science* 339(6117):296–300
Noack L, Breuer D. 2014. *Planet. Space Sci.* 98:41–49
Noack L, Rivoldini A, Van Hoolst T. 2017. *Phys. Earth Planet. Inter.* 269:40–57
Nortmann L, Pallé E, Salz M, et al. 2018. *Science* 362(6421):1388–91
Öberg KI, Murray-Clay R, Bergin EA. 2011. *Astrophys. J. Lett.* 743(1):L16
Odert P, Leitzinger M, Guenther EW, Heinzel P. 2020. *MNRAS* 494(3):3766–83
Oklopčić A, Hirata CM. 2018. *Astrophys. J. Lett.* 855(1):L11
Olson SL, Schwieterman EW, Reinhard CT, et al. 2018. *Astrophys. J. Lett.* 858(2):L14
Owen JE, Shaikhislamov IF, Lammer H, Fossati L, Khodachenko ML. 2020. *Space Sci. Rev.* 216(8):129
Owen JE, Wu Y. 2013. *Astrophys. J.* 775(2):105
Oze C, Sharma M. 2005. *Geophys. Res. Lett.* 32(10):L10203
Pierrehumbert R, Gaidos E. 2011. *Astrophys. J. Lett.* 734(1):L13
Pierrehumbert RT. 2010a. *Astrophys. J. Lett.* 726(1):L8
Pierrehumbert RT. 2010b. *Principles of Planetary Climate*. Cambridge, UK: Cambridge Univ. Press
Quanz SP, Ottiger M, Fontanet E, et al. 2021. arXiv:2101.07500 [astro-ph]
Rackham BV, Apai D, Giampapa MS. 2018. *Astrophys. J.* 853(2):122
Ramirez RM. 2018. *Geosciences* 8(8):280
Ramirez RM, Kaltenegger L. 2014. *Astrophys. J. Lett.* 797(2):L25
Ramirez RM, Levi A. 2018. *MNRAS* 477(4):4627–40
Ranjan S, Schwieterman EW, Harman C, et al. 2020. *Astrophys. J.* 896(2):148
Rannou P, McKay CP, Lorenz RD. 2003. *Planet. Space Sci.* 51(14/15):963–76
Rappaport S, Levine A, Chiang E, et al. 2012. *Astrophys. J.* 752(1):1
Raymond SN, Quinn T, Lunine JI. 2004. *Icarus* 168(1):1–17
Read PL, Tabataba-Vakili F, Wang Y, et al. 2018. *Q. J. R. Meteorol. Soc.* 144(717):2558–76
Ricker GR, Winn JN, Vanderspek R, et al. 2015. *J. Astron. Telesc. Instrum. Syst.* 1:014003
Rimmer PB, Rugheimer S. 2019. *Icarus* 329:124–31
Robinson TD, Catling DC. 2014. *Nat. Geosci.* 7(1):12–15
Robinson TD, Meadows VS, Crisp D. 2010. *Astrophys. J. Lett.* 721(1):L67
Rodler F, López-Morales M. 2014. *Astrophys. J.* 781(1):54
Rogers LA. 2015. *Astrophys. J.* 801(1):41
Rouan D, Deeg HJ, Demangeon O, et al. 2011. *Astrophys. J. Lett.* 741(2):L30
Rugheimer S, Kaltenegger L, Segura A, Linsky J, Mohanty S. 2015. *Astrophys. J.* 809(1):57
Schaefer L, Fegley B. 2009. *Astrophys. J. Lett.* 703(2):L113
Schaefer L, Lodders K, Fegley B. 2012. *Astrophys. J.* 755(1):41
Schaefer L, Sasselov D. 2015. *Astrophys. J.* 801(1):40
Schaefer L, Wordsworth RD, Berta-Thompson Z, Sasselov D. 2016. *Astrophys. J.* 829(2):63
Schlichting HE, Sari R, Yalinewich A. 2015. *Icarus* 247:81–94
Schwieterman EW, Kiang NY, Parenteau MN, et al. 2018. *Astrobiology* 18(6):663–708
Seager S. 2013. *Science* 340(6132):577–81
Seager S, Schrenk M, Bains W. 2012. *Astrobiology* 12(1):61–82
Segura A, Krelove K, Kasting JF, et al. 2003. *Astrobiology* 3(4):689–708
Segura A, Meadows VS, Kasting JF, Crisp D, Cohen M. 2007. *Astron. Astrophys.* 472(2):665–79
Selsis F, Despois D, Parisot JP. 2002. *Astron. Astrophys.* 388(3):985–1003
Selsis F, Kasting JF, Levrard B, et al. 2007. *Astron. Astrophys.* 476(3):1373–87
Selsis F, Wordsworth RD, Forget F. 2011. *Astron. Astrophys.* 532:A1
Sergeev DE, Lambert FH, Mayne NJ, et al. 2020. *Astrophys. J.* 894(2):84
Sheets HA, Deming D. 2017. *Astron. J.* 154(4):160
Shields AL, Ballard S, Johnson JA. 2016. *Phys. Rep.* 663:1–38
Shields AL, Meadows VS, Bitz CM, et al. 2013. *Astrobiology* 13(8):715–39

Shkolnik EL, Barman TS. 2014. *Astron. J.* 148(4):64
Showman AP, Polvani LM. 2010. *Geophys. Res. Lett.* 37(18)
Showman AP, Polvani LM. 2011. *Astrophys. J.* 738(1):71
Showman AP, Wordsworth RD, Merlis TM, Kaspi Y. 2013. *Comp. Climatol. Terr. Planets* 1:277–326
Sing DK, Fortney JJ, Nikolov N, et al. 2016. *Nature* 529(7584):59–62
Snellen I, de Kok R, Birkby JL, et al. 2015. *Astron. Astrophys.* 576:A59
Snellen IAG, de Kok RJ, de Mooij EJW, Albrecht S. 2010. *Nature* 465(7301):1049–51
Snellen IAG, de Kok RJ, le Poole R, Brogi M, Birkby J. 2013. *Astrophys. J.* 764(2):182
Snellen IAG, Guzman-Ramirez L, Hogerheijde MR, Hygate APS, Van der Tak FFS. 2020. *Astron. Astrophys.* 644:L2
Sousa-Silva C, Seager S, Ranjan S, et al. 2020. *Astrobiology* 20(2):235–68
Southworth J, Mancini L, Madhusudhan N, et al. 2017. *Astrophys. J.* 153(4):191
Suissa G, Mandell AM, Wolf ET, et al. 2020. *Astrophys. J.* 891(1):58
Swain MR, Estrela R, Roudier GM, et al. 2021. *Astrophys. J.* 161(5):213
Thompson MA, Telus M, Schaefer L, et al. 2021. *Nat. Astron.* 5(6):575–85
Tian F, France K, Linsky JL, Mauas PJD, Vieytes MC. 2014. *Earth Planet. Sci. Lett.* 385:22–27
Tian F, Ida S. 2015. *Nat. Geosci.* 8(3):177–80
Tian F, Kasting JF, Solomon SC. 2009. *Geophys. Res. Lett.* 36(2):L02205
Trainer MG, Pavlov AA, DeWitt HL, et al. 2006. *PNAS* 103(48):18035–42
Tsiaras A, Rocchetto M, Waldmann IP, et al. 2016. *Astrophys. J.* 820(2):99
Turbet M, Bolmont E, Ehrenreich D, et al. 2020. *Astron. Astrophys.* 638:A41
Turbet M, Leconte J, Selsis F, et al. 2016. *Astron. Astrophys.* 596:A112
Ugelow MS, De Haan DO, Hörst SM, Tolbert MA. 2018. *Astrophys. J. Lett.* 859:L2
Unterborn CT, Desch SJ, Hinkel NR, Lorenzo A. 2018. *Nat. Astron.* 2(4):297–302
Unterborn CT, Kabbes JE, Pigott JS, Reaman DM, Panero WR. 2014. *Astrophys. J.* 793(2):124
Valencia D, Ikoma M, Guillot T, Nettelmann N. 2010. *Astron. Astrophys.* 516:A20
Valencia D, O'Connell RJ, Sasselov DD. 2007. *Astrophys. J. Lett.* 670(1):L45
Van Eylen V, Agentoft C, Lundkvist MS, et al. 2018. *MNRAS* 479(4):4786–95
Waalkes WC, Berta-Thompson Z, Bourrier V, et al. 2019. *Astron. J.* 158(1):50
Walker JCG, Hays PB, Kasting JF. 1981. *J. Geophys. Res. Oceans* 86(10):C9776–82
Wang H, Wordsworth R. 2020. *Astrophys. J.* 891(1):7
Wang Y, Read PL, Tabataba-Vakili F, Young RMB. 2018. *Q. J. R. Meteorol. Soc.* 144(717):2537–57
Watson AJ, Donahue TM, Walker JCG. 1981. *Icarus* 48(2):150–66
Weiss LM, Marcy GW. 2014. *Astrophys. J. Lett.* 783(1):L6
Williams CD, Mukhopadhyay S. 2019. *Nature* 565(7737):78–81
Wolf ET. 2017. *Astrophys. J. Lett.* 839(1):L1
Wolfgang A, Lopez E. 2015. *Astrophys. J.* 806(2):183
Wordsworth RD. 2012. *Icarus* 219(1):267–73
Wordsworth RD. 2015. *Astrophys. J.* 806(2):180
Wordsworth RD. 2016a. *Earth Planet. Sci. Lett.* 447:103–11
Wordsworth RD. 2016b. *Annu. Rev. Earth Planet. Sci.* 44:381–408
Wordsworth RD. 2021. *Astrophys. J. Lett.* 912(1):L14
Wordsworth RD, Forget F, Selsis F, et al. 2011. *Astrophys. J. Lett.* 733(2):L48
Wordsworth RD, Kalugina Y, Lokshtanov S, et al. 2017. *Geophys. Res. Lett.* 44(2):665–71
Wordsworth RD, Pierrehumbert R. 2013a. *Science* 339(6115):64–67
Wordsworth RD, Pierrehumbert R. 2013b. *Astrophys. J.* 778(2):154
Wordsworth RD, Pierrehumbert R. 2014. *Astrophys. J. Lett.* 785(2):L20
Wordsworth RD, Schaefer LK, Fischer RA. 2018. *Astron. J.* 155(5):195
Wunderlich F, Godolt M, Grenfell JL, et al. 2019. *Astron. Astrophys.* 624:A49
Yang J, Cowan NB, Abbot DS. 2013. *Astrophys. J. Lett.* 771(2):L45
Yu X, Moses JI, Fortney JJ, Zhang X. 2021. *Astrophys. J.* 914(1):38
Yung YL, DeMore WB. 1999. *Photochemistry of Planetary Atmospheres*, Vol. 1. Oxford, UK: Oxford Univ. Press

Zahnle K, Kasting JF, Pollack JB. 1990. *Icarus* 84(2):502–27
Zahnle K, Pollack JB, Grinspoon D, Dones L. 1992. *Icarus* 95(1):1–23
Zahnle KJ, Catling DC. 2017. *Astrophys. J.* 843(2):122
Zahnle KJ, Catling DC, Claire MW. 2013. *Chem. Geol.* 362:26–34
Zahnle KJ, Lupu R, Catling DC, Wogan N. 2020. *Planet. Sci. J.* 1(1):11
Zahnle KJ, Walker JC. 1982. *Rev. Geophys.* 20(2):280–92
Zeng L, Jacobsen SB, Sasselov DD, et al. 2019. *PNAS* 116(20):9723–28
Zerkle AL, Claire MW, Domagal-Goldman SD, Farquhar J, Poulton SW. 2012. *Nat. Geosci.* 5(5):359–63
Zhang M, Knutson HA, Wang L, et al. 2021. *Astrophys. J.* 161(4):181
Zhang X, Strobel DF, Imanaka H. 2017. *Nature* 551(7680):352–55
Zolotov MY. 2018. *Rev. Mineral. Geochem.* 84(1):351–92
Zsom A, Kaltenegger L, Goldblatt C. 2012. *Icarus* 221(2):603–16

Annual Review of Astronomy and Astrophysics
Volume 60, 2022

Contents